C Journal of Carbon Research

MDPI

Review

Fused Deposition Modelling of Thermoplastic Polymer Nanocomposites: A Critical Review

Taha Sheikh * and Kamran Behdinan *

Advanced Research Laboratory for Multifunctional Lightweight Structures (ARL-MLS), Department of Mechanical & Industrial Engineering, University of Toronto, Toronto, ON M6B 1Y8, Canada
* Correspondence: t.sheikh@mail.utoronto.ca (T.S.); behdinan@mie.utoronto.ca (K.B.)

Abstract: Fused deposition modelling (FDM) has attracted researchers' interest in myriads of applications. The enhancement of its part using fillers to print nanocomposites is a cutting-edge domain of research. Industrial acceptance is still a challenge, and researchers are investigating different nanofillers and polymer matrix combinations to investigate FDM-printed nanocomposites. Carbon nanotubes, graphene, and cellulose are heavily studied nanofillers because of their astonishing properties, biocompatibility, and ability to tailor the final performance of the FDM-printed nanocomposite part. This work presents a comprehensive review of polymer nanocomposites based on these nanofillers. Important examples, case studies, and results are discussed and compared to elaborate the understanding of the processing of nanocomposites, filaments, printing, and the characterisation of these nanocomposites. A detailed and exhaustive discussion of the prospective computational models, with challenges and a future road map, is provided, enabling the scientific community to understand these nanocomposites and their FDM processing for wider industrial applications and acceptance.

Keywords: additive manufacturing; fused deposition modelling; computational modelling; polymer nanocomposites; feedstock filament

Citation: Sheikh, T.; Behdinan, K. Fused Deposition Modelling of Thermoplastic Polymer Nanocomposites: A Critical Review. *C* **2024**, *10*, 29. https://doi.org/10.3390/c10020029

Academic Editors: Chi-Hui Tsou and Patrizia Savi

Received: 4 February 2024
Revised: 12 March 2024
Accepted: 13 March 2024
Published: 25 March 2024

1. Introduction

Fused deposition modelling (FDM), developed by Stratasys in 1989, is an additive manufacturing (AM) technology that has a global market share of 40% [1]. AM started around 1980 with the first patent for stereolithography (SLA) [2]. SLA is a process that is different from FDM in terms of material use and the energy required for the processing of materials. In SLA, liquid resins are used as inputs or raw materials, which are then solidified via ultraviolet light. The FDM process involves the melting of filaments followed by their extrusion as rasters and subsequent layers. Fused deposition modelling can be used to rapidly manufacture materials of complex sizes and geometries, reducing cost and time investments [3–7]. FDM's advantages over conventional manufacturing methods, such as extrusion or injection moulding, are reasons why it has attracted the interest of researchers [8,9]. This has made FDM an emerging candidate in the production industry, with a current projected cumulative annual growth rate (CAGR) of 21% for the period of 2022–2030 [10]. Its development has increased the demand for its application in various sectors, such as medicine, biomedicine, automotive, aerospace, and construction [11–14]. FDM, also referred to as fused filament fabrication (FFF), provides the real-time manufacturing of complex shapes with cost-effectiveness. The method utilises a simple layer-by-layer technique of depositing molten material to fabricate a complete part. The most popular materials include polymers such as polylactic acid (PLA), acrylonitrile–butadiene–styrene (ABS), polyethylene (PE), polycarbonate (PC), polyethylene terephthalate (PET), thermoplastic urethane (TPU), polyether–ether-ketone (PEEK), and nylon [14–18]. Despite the advantages of this technique, the final printed parts lack in performance compared to the parts derived from conventional manufacturing methods such as injection moulding. Many

process parameters, such as layer height, raster orientation, infill density, and many more, have been studied to determine how they affect the final product's properties [15,19–23]. For improving performance, it is also reported that the input feedstock material, in the form of a filament, affects the print quality because of its characteristics. The FDM process involves the melting of filaments, followed by their extrusion as rasters and subsequent layers. Therefore, the solidification time (curing) and temperature also play vital roles in controlling the printed part's performance. This has motivated researchers to find solutions, and consequently, composites have become a topic of research interest. Carbon fibres (short, continuous), single-walled and multi-walled carbon nanotubes (SWCNTs/MWCNTs), graphene, and carbon black have been popular materials to study. Other choices, such as natural fibres (jute, bamboo, coconut, and husk), metals, and their nanofillers, have also attracted interest [24–26].

This study presents a detailed discussion of CNT, graphene, and cellulose-based nanocomposites, together with case studies discussing the characterisation and effect of these fillers on the final performance of FDM parts. There are many recent review articles in the literature focusing on FDM and its process, parameters, and materials. Ahmad et al. [27] discussed natural fibre-reinforced thermoplastic composites for FDM. Their short review details the rheological properties, processing, and effect of these fillers on the polymer matrix in the FDM method but is only restricted to one class of materials, with no discussion on nanofillers, and Almuallim et al. [28] reviewed composite materials only for thermal conductivity applications. The authors reviewed metallic and carbon-based non-metallic fillers. Their study did not discuss any of the computational techniques used to characterise the printed parts, and its discussion was also restricted because of the authors' vast filler choices. Sandanamsamy et al. [29] presented a detailed review work focusing on the PLA material matrix only. This is an interesting but limited work since the myriad materials available that demonstrate excellent properties when combined with nanofillers were not discussed. Parnian et al. [30] produced a detailed review work only focusing on CNTs as nanofillers, and Roudny et al. [31] also restricted their discussion to thermal conductive applications. Park et al. [32] presented a detailed article in which they mainly discussed matrix materials and fillers for different application areas in additive manufacturing. Penumkala et al. [19] also presented a similar study focused on thermoplastic polymer composites. These investigations are detailed and present a complete picture of the composites used in FDM, but because of the large volume of content to discuss, many recent and important studies have been missed.

The present work is focused on presenting the recent advancements and challenges in processing the CNT, graphene, and cellulose nanofillers in the polymer matrix for FDM. The effects of such fillers on the final properties of printed products are discussed and compared with important findings and challenges. Furthermore, a detailed, exhaustive discussion is presented, along with a conclusion discussing the future roadmap for nanocomposites and possible solutions to the challenges associated with these nanocomposites. One important aspect of this study is its discussion of computational models, which is of the utmost necessity because studies on such FDM-printed nanocomposites are missing from the literature. This paper is organised as follows: In Section 2, the fundamentals of the FDM process are discussed, along with feedstock filament processing. This is followed by a discussion of CNT, graphene, and cellulose nanocomposites in Section 3. The paper concludes with a holistic, detailed discussion and conclusion in Sections 4 and 5, respectively.

2. FDM Process

The schematic of FDM is shown in Figure 1a, a wired filament passing through an extruder heated, melted, and extruded through a nozzle opening and deposited on a surface. Though the process is simple, there are many parameters and challenges governing the entire FDM technique. Focusing on the initial stage, i.e., filaments, the parameters such as the filament diameter, glass transition temperature (T_g), processing temperature, and rheology of the polymer are very important to be controlled. The FDM printers are

generally standardised for a diameter of 1.75 mm or 2.85 mm [33]; therefore, the diameter of the filament needs to be consistent to be continuously fed into the printer, either in a direct head extruder (which feeds the filament directly into nozzle) or via a Bowden tube (a plastic tube is used to guide the filament into extruder). Another issue with inconsistent diameter is that, even if it passes into the extruder and manages to come out of the nozzle, the flow rate of output will be altered, hence the deposition of material, finally deteriorating the final part. The extruder melting temperature should be carefully controlled; if the temperature is too high, it will deteriorate the polymer, and when too low, it will not melt [34]. Once the filament is melted, the molten mix is pushed out of the nozzle, inducing a shear effect between the nozzle wall and the molten mix. The inlet diameter will be larger (1.75 or 2.85 mm) than the outlet diameter (about 0.3–0.8 mm); this induces the shear and elongation flow. Therefore, the molten mix must demonstrate shear thinning behaviour; at a low shear rate, the viscosity should be high to prevent premature extrusion, and for a high shear rate, the viscosity must decrease to allow the molten mix to pass through the nozzle [35]. In the literature, it has not been quantified what should be the range of viscosity for a proper filament of the FDM process [36]. The reason is that it is extremely difficult to measure the actual or exact shear stress during the printing of polymer. Another factor that affects the viscosity is the die swell at the exit of the nozzle. For low viscosity at a high shear rate, the polymer molecules move rapidly, lowering the high elastic energy and reducing the die swell. With a high shear stress region (near the small area of the nozzle), the polymer chains tend to align themselves, which is reversed when the chains tend to go back to their initial state. This happens because after exiting the nozzle, the diameter of the molten mix is increased, and cooling takes place by the heat transfer mechanism. Therefore, it is of utmost importance to understand and characterise the polymer material before processing it in the FDM method. Once this stage is completed, the molten polymer is deposited layer over layer to complete the print. Several factors, such as the process parameters (layer height, raster orientation, etc.), bed temperature, printing speed, and ambient temperature (controlling the heat transfer between the melted polymer and environment), etc., control the print quality [37]. The next section discusses the important factors and parameters in filament feedstock of the FDM method when processing nanofillers.

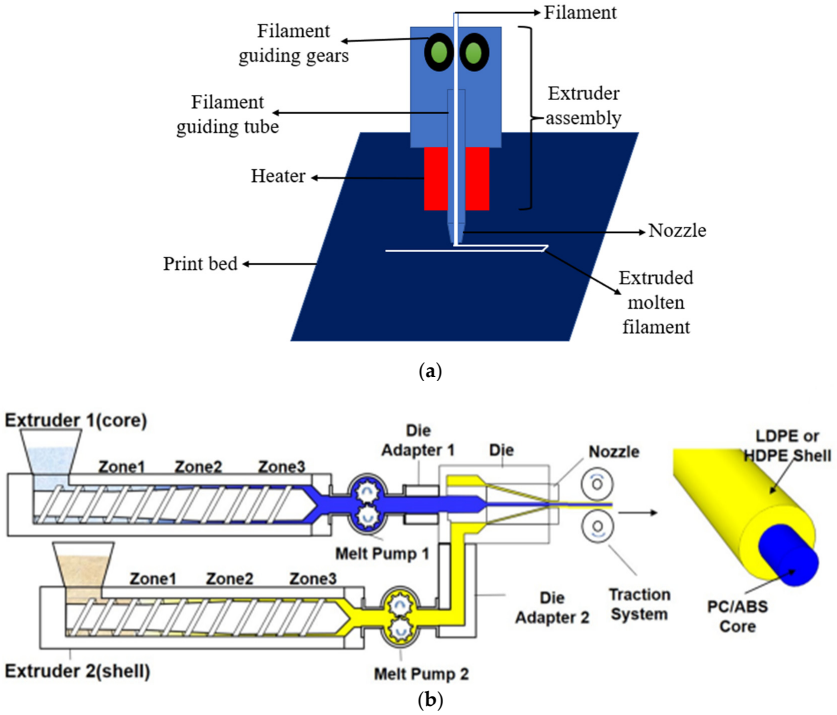

Figure 1. (**a**) Schematic representation of the FDM method. (**b**) Schematic of core–shell filament processing [38].

2.1. FDM Filament Production

The most common filament materials because of printability, visual quality, and mechanical properties are polylactic acid (PLA), acrylonitrile–butadiene–styrene (ABS), polycarbonate (PC), nylon (PA), and polyethylene terephthalate (PET). To improve the final performance of the printed parts with these materials, researchers blended polymers with fillers as composite materials. These materials or structures are referred to as multi-material/structure filaments and are mostly used as core–shell filaments [38]. Such a class of filaments comprises one core material and one shell. To process these into filaments, two single-screw extruders, one as the core and the other as the shell, are used simultaneously. Both these extruders are attached to a common circular die opening, combining the two separate materials into one filament, as shown in Figure 1b. The main objective to create core–shell filaments is to improve the final properties of the FDM parts, such as print quality, fracture toughness, and impact resistance. Also, when printing semi-crystalline polymers, it is very difficult to achieve a high print quality due to the large volume change in crystallisation [39]. A study reported that to improve the toughness, the core–shell manufacturing technique was employed. PC/ABS, together with high-density polyethylene (HDPE) or low-density polyethylene (LDPE), was used as the core and shell materials, respectively. The resulting filament had high toughness because of the low ductility of polyethylene. Another method, termed as the thermal drawn method, is reported in the literature to create core–shell filaments [40]. There are other composite filaments, continuous fibre polymer composites, and short fibre polymer composites, which are not discussed because they are beyond the scope of this work and can be referred to [19,41] for details.

To increase the ease of printing and improve the final performance, scientists have turned towards nanocomposite materials [42–44]. Thermoplastic polymers such as PLA, ABS, or others have been used as the matrix with nanoparticles such as graphene, carbon nanotubes, and others to create printable filaments. In general, the chemical solution method (solution casting) or mechanical processing (melt processing) method is employed to create nanocomposite filaments. The former produces better dispersion and less agglomeration of nanoparticles than the latter. However, mechanical processing is quite simple and easy to carry out. The methods are detailed below graphically and textually.

2.2. Chemical Solution Method

This method involves chemical treatment to produce the filament. A solvent is used to disperse the nanoparticles, which are sonicated for some time. The main objective of sonication is to increase the dispersion, which reduces the agglomeration of nanoparticles together. If the nanoparticles agglomerate heavily, it induces the stress concentration in the final composite and reduces the mechanical strength of the part [45]. The next step involves the preparation of the polymer matrix solution. One way is by directly dissolving the polymer into the nanoparticle solution or preparing a separate polymer solution and then mixing it. The former method reduces extra steps and requires less solvent, but the latter will ensure proper dissolution of solid polymer in solvent. Care must be taken for selecting the polymer for dissolution; the best to use is the powdered form of polymer or small-size pellets. The polymer–nanoparticle solution should be mixed well using a magnetic stirrer for a couple of hours. Once a homogeneous nanocomposite solution is obtained, thin sheets are prepared, which will allow the solvent to evaporate. These sheets are further shredded or pelletized to prepare to extrude the nanocomposite for filament making. The following points must be taken care of: (i) The selection of solvent and the chemistry of the solvent with nanoparticles and polymer must be known. Otherwise, the chemical reaction between the solvent–nanoparticles or solvent–polymer will change or deteriorate the final composite material. (ii) The pellets or shredded nanocomposite particles must be heated in an oven (convection or vacuum) for a very long time to remove as much solvent as possible. Chemical solution methods have been reported heavily in the literature. Podsiadly et al. [46] prepared ABS-CNT filaments, dispersing CNTs in acetone and sonicating for 20 min. The authors mixed the polymer–CNT mix for about 5 h, and the sheets were dried overnight to

evaporate the solvent. One interesting method of preparing the nanocomposite filament is the local enrichment method. This method has not been reported substantially and needs further investigation. Shi et al. [47,48] prepared the PLA-CNT nanocomposites by coating the PLA filament with a CNT thin layer. The process is shown in Figure 2, which details the layer preparation on PLA filament using chemicals. The prepared nanocomposite filament later, when characterised, showed excellent improvement in the properties of FDM prints.

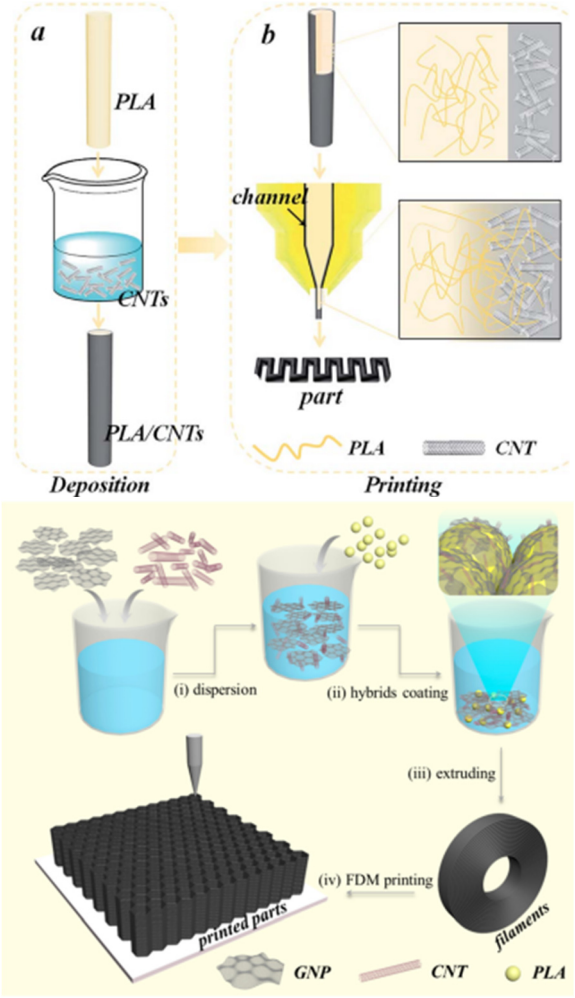

(**c**)

Figure 2. (**a**) Local enrichment process of coating filament with nanofillers. (**b**) FDM printing of the coated nanocomposite. (**c**) Local enrichment using two nanofillers (CNTs and graphene) [47,48].

2.3. Mechanical Processing

To create a nanocomposite, an extruder is used to mix the nanoparticles and polymer matrix. Before mixing, the materials should be dried if they have a hygroscopic nature to remove any traces of moisture. A high rotation rate is employed near 90–100 rpm to produce high shearing for better mixing and the dispersion of nanoparticles. The final nanocomposite is converted into powder, pellets, or shredded for filament extrusion. To achieve as much homogeneity as possible, Dul et al. [49,50] mixed CNTs with ABS polymer in a counter-rotating mixer at 190 °C at 90 rpm for 15 min. Later, the prepared nanocomposite was granulated and processed for filament into the extruder, as shown in Figure 3a for the MWCNTs and SWCNTs [49]. Jing et al. [51] used a shear pan-milling mixer to mix the low-density polyethylene (LLDPE) with graphene nanoparticles, as shown in Figure 3b. The cycles were repeated four times to obtain a homogeneous mixture of the nanofillers and polymer matrix. To dissipate the heat generated, an internal water-

cooling system was installed in the miller. Huang et al. [52] prepared a dual matrix CNT nanocomposite using the melt-mixing method, as shown in Figure 3c,d. The authors used a mixer rate of 750 rpm for about 1 h to mix TPU and PLA. Further, the MWCNTs were added in the required proportion and mixed for 2 h. Before processing the nanocomposite mix, it was dried for about 8 h to remove any traces of moisture that could hinder the surface quality and diameter tolerance of the filament. Figure 3e shows the morphology of the prepared nanocomposite filament, which shows that both polymer matrices are in phase separation, and the CNTs are distributed evenly but in agglomerated form.

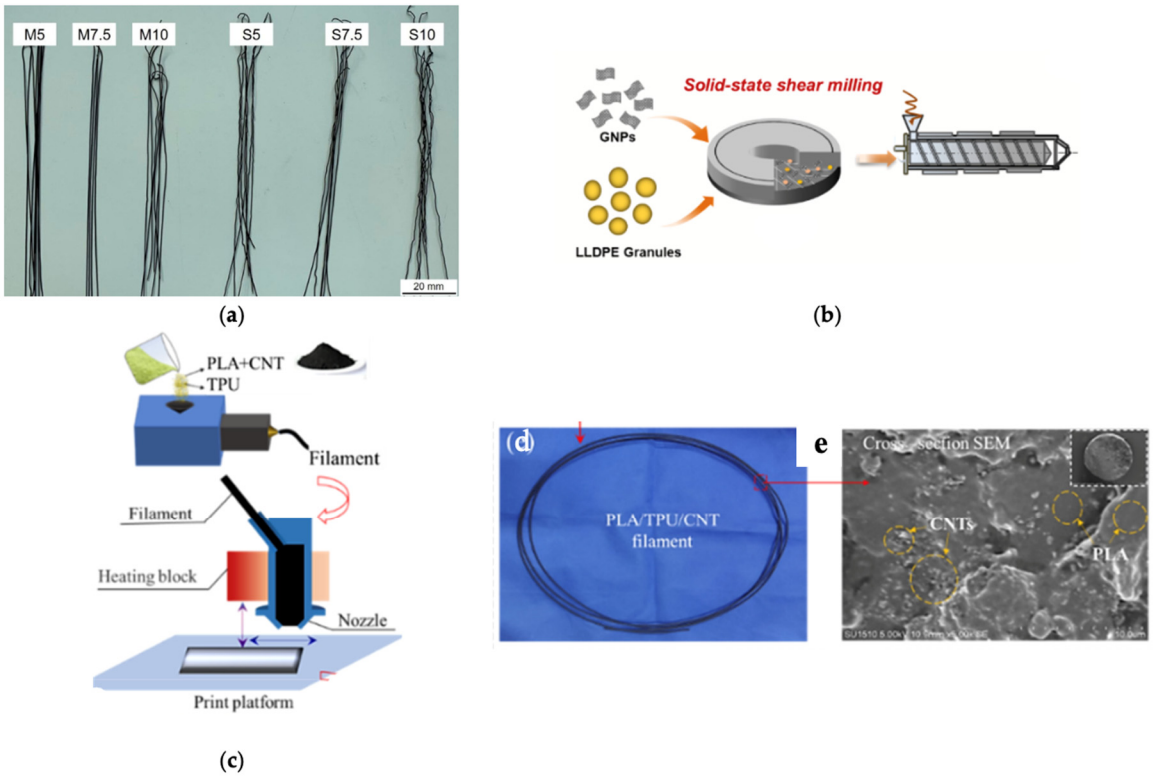

Figure 3. (**a**) SWCNT (S) and MWCNT (M) nanocomposite filaments [49]. (**b**) Mechanical mixing (melt-mixing) process to fabricate nanocomposite [51]. (**c**) PLA/TPU/CNT nanocomposite filament fabrication and printing using FDM. (**d**,**e**) Prepared filament and SEM images showing the dispersed phases of the matrix and nanofiller [52].

2.4. Extrusion

The nanocomposite as pellets or granules are fed into an extruder machine with a die opening of the required filament diameter. In general, 1.75 mm and 2.85 mm are preferred for nanocomposite filament because most FDM printers use this setting. The higher diameter filament could be processed depending on the type of printer in use. The choice of the extruder is independent, and the literature reports some extruders with die openings as the filament final diameter and then using water- and air-cooling systems. The basic principle of the extruding filament is that, firstly, the granulated polymers are dried and fed into the feedstock hopper, which is melted into the heated chamber of the screw. The polymer melt is homogeneously mixed here while passing through the heated barrel via the screw. Finally, this melt is pushed out of a die opening where the filament is cooled (water or air) and wounded over a spool. The entire process is schematically represented in Figure 4. This melt processing of polymer into filament is affected by several controlling parameters that affect the filament homogeneity [53]. Especially for composite filaments, the extrusion process controls the orientation of the fillers in the final filament [54]; such CNTs tend to orient in the direction of extrusion [55]. The process parameters, such as the feed rate, temperature, speed of the screw, and pulling speed of the filament, can

be controlled to control the filament printability. The two types of extruders used, the single screw and double screw (twin), differ in the number of rotating screws inside the barrel. The single-screw extruder is simple, offering a low cost and maintenance, but since it only has one screw, good mixing is a challenge [56]. The rotation of the screw causes friction between the barrel surface and the screw, causing the melt to pass through the opening die [57]. However, single-screw extruders possess one challenge: Upon increasing the rotational speed, high thermal energy is generated because of the increased friction forces, making it unsuitable for heat-sensible polymers. For the extrusion of composites, proper homogeneous mixing is a challenge because of the single screw producing low shear. Therefore, twin- or double-screw extruders could be used. The two parallel screws to the barrel produce high shear and better and homogeneous mixing of the polymers or matrix-fillers [53]. Another advantage of the twin-screw extruder is that the direction of the screw's rotation can be controlled. For better mixing of the filler particles, opposite rotation of the screws (counter-rotation) proves to be effective in comparison to co-extrusion (same direction rotation) because the counter-rotation produces more shear forces [58,59].

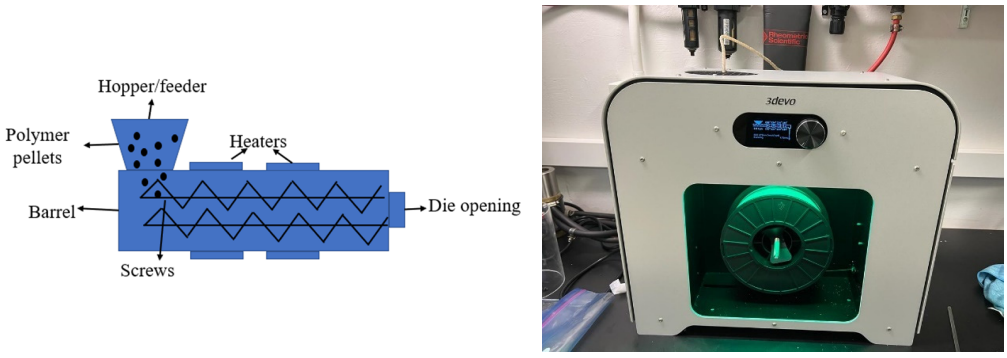

(**a**) (**b**)

Figure 4. (**a**) A schematic representation of twin (double)-screw extruders. (**b**) Filament extruder from 3devo Ltd.

For automation, complete automated extruders are designed especially for FDM filament production, such as the composer by 3devo Ltd. (Utrecht, The Netherlands) [60], detailed in Figure 4b. The extruder is very simple to use and does not require any specific knowledge of the process. It comes with a hopper to input pellets of about 0.4 mm in size (a high size would affect the filament diameter). The single screw heated by four heating zones ensures the uniform heating of the melt inside the screw. A downward vertical opening guides the melt (cooled by twin fans) through an optical sensor-controlled wheel. This wheel ensures the consistency of the desired filament diameter, which is collected over a rotating spool. This is just one good extruder available for FDM filament; there are multiple nowadays on the market, and they can be chosen according to one's budget and necessity. The factors to be taken care of are (i) the consistent diameter of the filament, which is difficult to achieve in one extrusion. Therefore, the extrusion process must be repeated multiple times to attain consistency in the filament diameter. (ii) The temperature profile for a new nanocomposite material must be selected by hit and trail for consistent filaments free from any lumps or porosity.

3. Filler Types

3.1. Carbon Nanotube Polymer Nanocomposite

Carbon nanotubes have demonstrated excellent properties, such as their low density and thermal, mechanical, and electrical properties [31,61,62], for vast applications such as sensors, energy storage, etc. [63,64]. In comparison to conventional manufacturing methods, such as casting or coating the structure with nanofillers, additive manufacturing offers low costs and rapid fabrication in real time [65,66]. Oran et al. [67] investigated multi-walled carbon nanotube (MWCNTs)-ABS nanocomposites printed via FDM for morphology,

electrical, and mechanical properties. The author reported the optimum temperature and loading ratio as 250 °C and 10% by weight. The nanoparticle and polymer matrix physical interaction increases with the nanoparticle content, which increases the viscosity of the nanocomposite [68]. As shown in Figure 5, the melt flow index (MFI) decreases significantly with the CNT content.

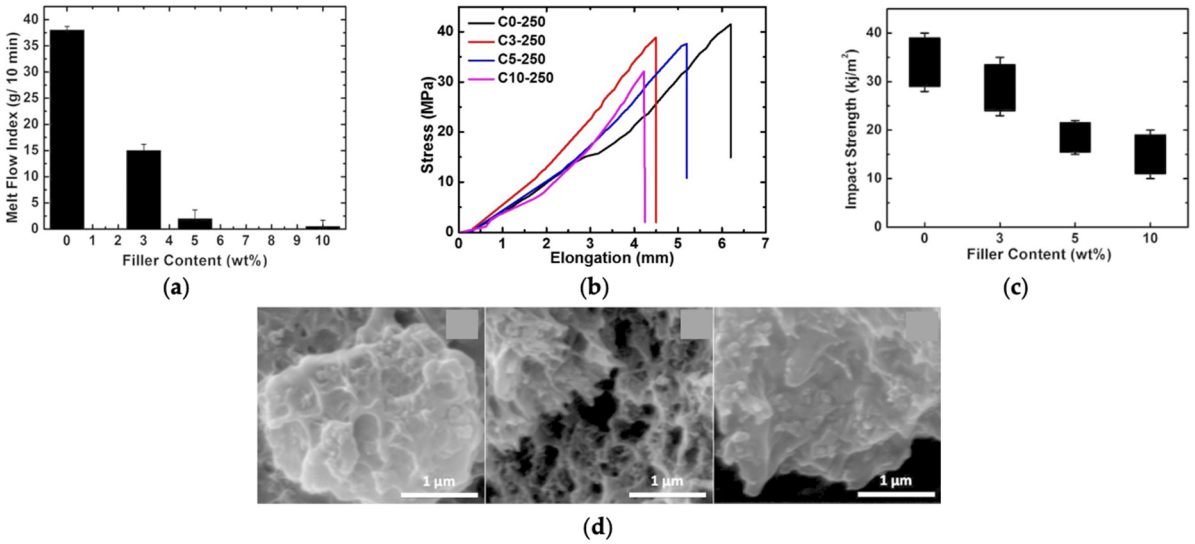

Figure 5. (**a**–**c**) MFI, stress–strain measure, and impact strength are affected by CNTs in ABS polymer, respectively. (**d**) Electronic images of prepared nanocomposites [67].

Scanning electron microscopy was used by the authors to investigate the morphology of the nanocomposites, as shown in Figure 5d. The foam-like porous morphology is reported because of the CNT agglomeration in the nanocomposite. The average size of 1 µm was calculated, which is associated with the better mixing efficiency of the extruder. This signifies that for better dispersion, the extrusion process should be repeated multiple times. Another detrimental effect of agglomeration is represented in Figure 5b. The elastic modulus increased for the 3% CNT concentration in the polymer matrix and then decreased because of the entanglement of nanotubes among themselves. The impact strength decreases upon dispersing the rigid nanoparticles in a tough polymer matrix [69,70].

Le et al. [71] experimentally characterised the MWCNT-ABS nanocomposite parts. The authors prepared 0.5%, 1%, 1.5%, 2%, 3%, and 4% by weight MWCNT-ABS samples and analysed the morphology and mechanical properties experimentally. The morphology analysis produced significant findings, reporting that the fracture surface exhibited less shear lip and few voids for the lower nanofiller content, but the shear lips increased with voids, as shown in Figure 6, upon increasing the nanofillers content. The tensile test demonstrated that for 2 wt% CNTs, a 40% increase in tensile strength can be achieved compared to the neat ABS.

Wang et al. [72] studied the effect of nanoparticles on material printability and adhesion quality. Upon dispersion of CNTs in the ABS matrix, the nanoparticles generally disperse into styrene–acrylonitrile (SAN) than the polybutadiene (PB) phase. Figure 7a shows the electron microscopic image of a 5 wt% nanocomposite sample with PB in spheres. Upon comparing the neat ABS with the nanocomposite sample, it is reported that the adhesion area and voids were almost similar. Therefore, a conclusive remark was suggested that until 8 wt%, the adhesion and printability of the material do not change relative to neat polymer. The porosity analysis showed that for a small concentration of up to 8 wt%, the printed parts demonstrate the same porous concentration as of neat polymer. But, besides these unaffected properties, mechanical properties showed significant improvement. The author reported a 10.25% and 40% increase in the modulus for the 1 wt% and 8 wt% samples relative to the neat ABS, respectively, as shown in Figure 7b.

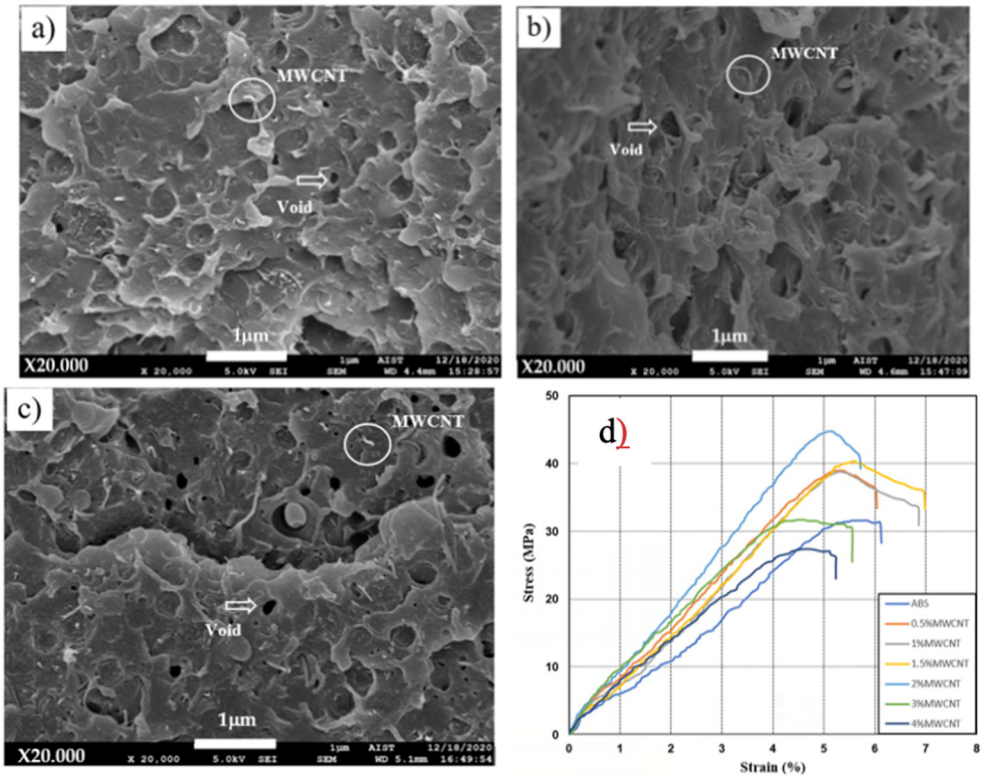

Figure 6. Morphology of MWCNT and ABS nanocomposites (**a**–**c**). (**d**) Stress–strain graph of the prepared nanocomposite [71].

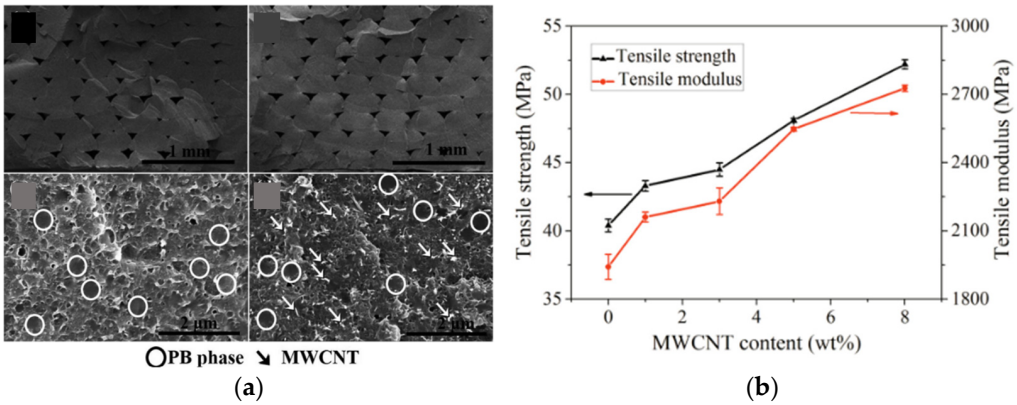

(**a**) (**b**)

Figure 7. (**a**) SEM images of the nanocomposite showing dispersed phases. (**b**) Tensile strength is affected by the CNTs [72].

Podsiadly et al. [48] characterised the FDM-printed CNT-reinforced ABS nanocomposite parts for their electrical and mechanical properties. The mechanical results demonstrated that the nanoparticles in the polymer matrix resulted in a decrease in ultimate tensile strength up to 5 wt%; after that, it increased. Below the 9 wt% threshold, the nanoparticles demonstrate less entanglement in their structure, thereby decreasing the cross-sectional area of the polymer and finally reducing the tensile strength. If the concentration is increased, the entanglement increases, and hence the mechanical strength as well [73,74]. The electrical conductivity was measured in terms of resistivity. For lower concentrations < 2 wt%, the FDM parts were almost nonconductive (200 M Ωm). Upon increasing the CNT content, the resistivity showed a decreasing effect; for 4.76 wt%, a resistivity of 2.5 Ωm was obtained, and for 9 wt%, the resistivity was further reduced to 0.15 Ωm. This is because, for a lower nanoparticle content, the conductive path is not complete or continuous in comparison to a higher content, as shown in Figure 8. Figure 8

shows the tunnelling effect in FDM-printed nanocomposites. The current–voltage (I–V) characteristics for the threshold content demonstrated a non-linear decreasing behaviour in resistance upon increasing the voltage. The physics behind this phenomenon could be interpreted as, with an increase in electrical current the temperature also increases, which decreases the resistance of FDM-printed nanocomposites for higher voltages. The CNT-based nanocomposites were reported as negative temperature coefficient (NTC) resistive. It means that electrical resistivity is inversely proportional to the current [75–77]. In conclusion, the electrical percolation threshold could be estimated at around 4.76 wt% and mechanical to be 9 wt%.

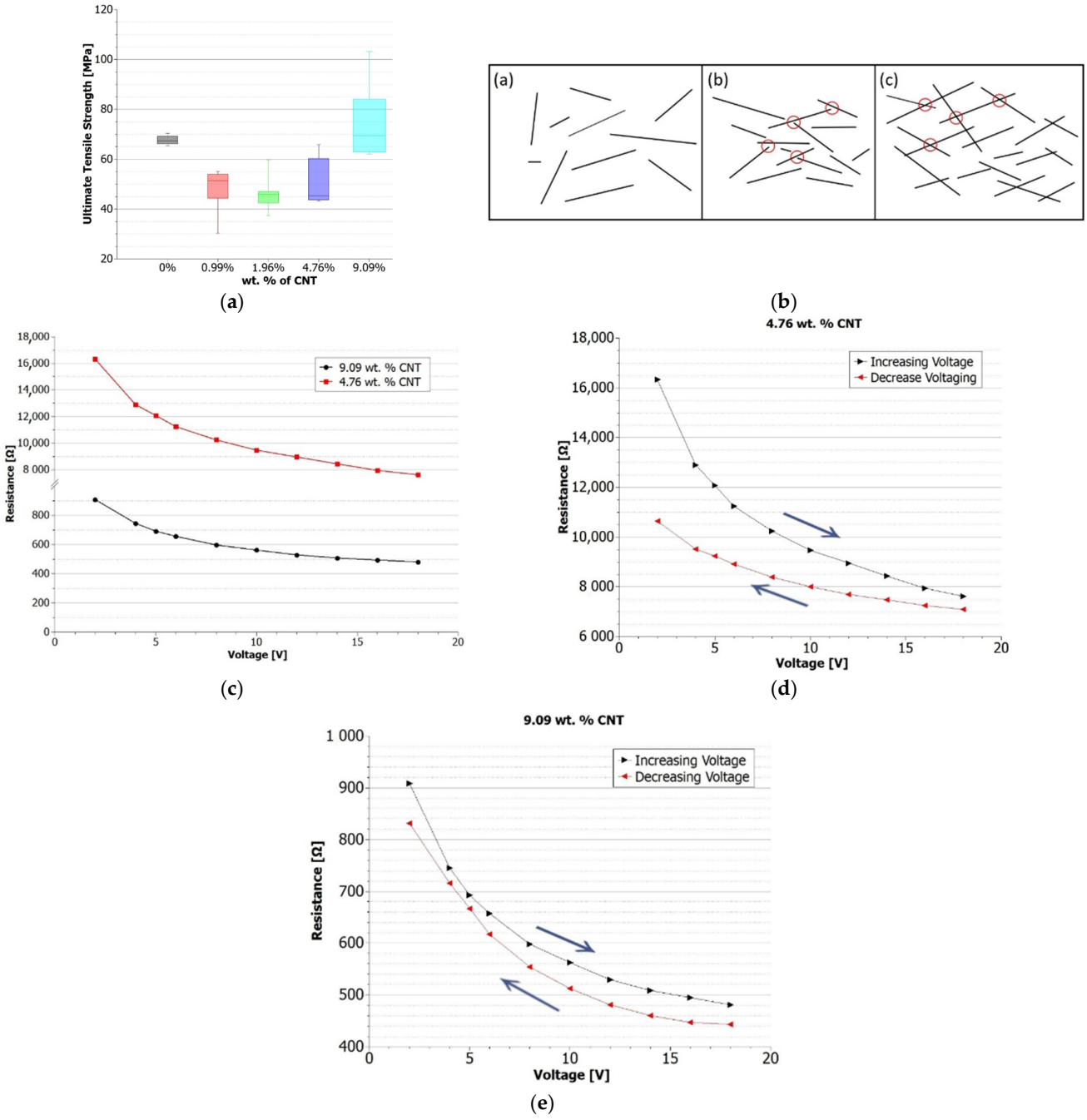

Figure 8. (**a**) Ultimate tensile strength variation with CNT content. (**b**) CNT percolation in ABS polymer matrix. (**c**) Electrical resistance variation for different CNT contents. (**d**,**e**) Effect of CNTs on resistance for increasing and decreasing voltages [48].

Some other studies were also reported while considering CNT-ABS nanocomposites, investigating their electrical and mechanical properties. Sezer et al. [78] studied, for the first time, 10 wt% MWCNT-ABS FDM-printed nanocomposite and reported 210% increases in the ultimate tensile strength. Improvement in electrical properties, as shown in Figure 9, was also observed. The authors also analysed the effect of raster orientation on the mechanical properties and electrical properties of such nanocomposites. The parts printed with a 45–45-degree raster shows lower properties when compared to 0–90 because of the CNT path discontinuity resulting from crossed layers. From this experimental analysis, it is evident that for the lower CNT content, the properties are not improved very much because of the agglomeration of CNTs. The mechanical threshold in most of the studied literature is reported to be around 9–10 wt%. The electrical conductivity because of the tunnelling effect is of the NTC type. For higher CNT contents, the resistivity decreases very substantially and was reported in the practical application domain. In another work, Pan et al. [79] prepared a polyphenylene sulphide (PPS)-CNT nanocomposite and investigated the mechanical and tribological properties. The printed nanocomposite demonstrated an increase of 26% and 29% in its tensile and bending strengths. The studies only focussed on the experimental characterisation of the FDM nanocomposite samples with the maximum CNT content reported to be 10 wt%. The challenges for higher concentrations were related to higher agglomeration, poor dispersion, nozzle clogging, higher brittle nature of the composite, and poor ductility [80]. Other polymer matrices have been studied with CNTs using the FDM method. High-density polyethylene/MWCNTs 3D-printed nanocomposites were investigated for their thermal properties compared to conventional plain polymers [81]. Han et al. [82] investigated MWCNTs dispersed in polyamide 12 polymer-printed parts for the electromagnetic wave absorption properties. The authors selected the 7 wt% to 12 wt% concentration of carbon nanotubes because the literature reported poor electrical properties for less CNT concentration.

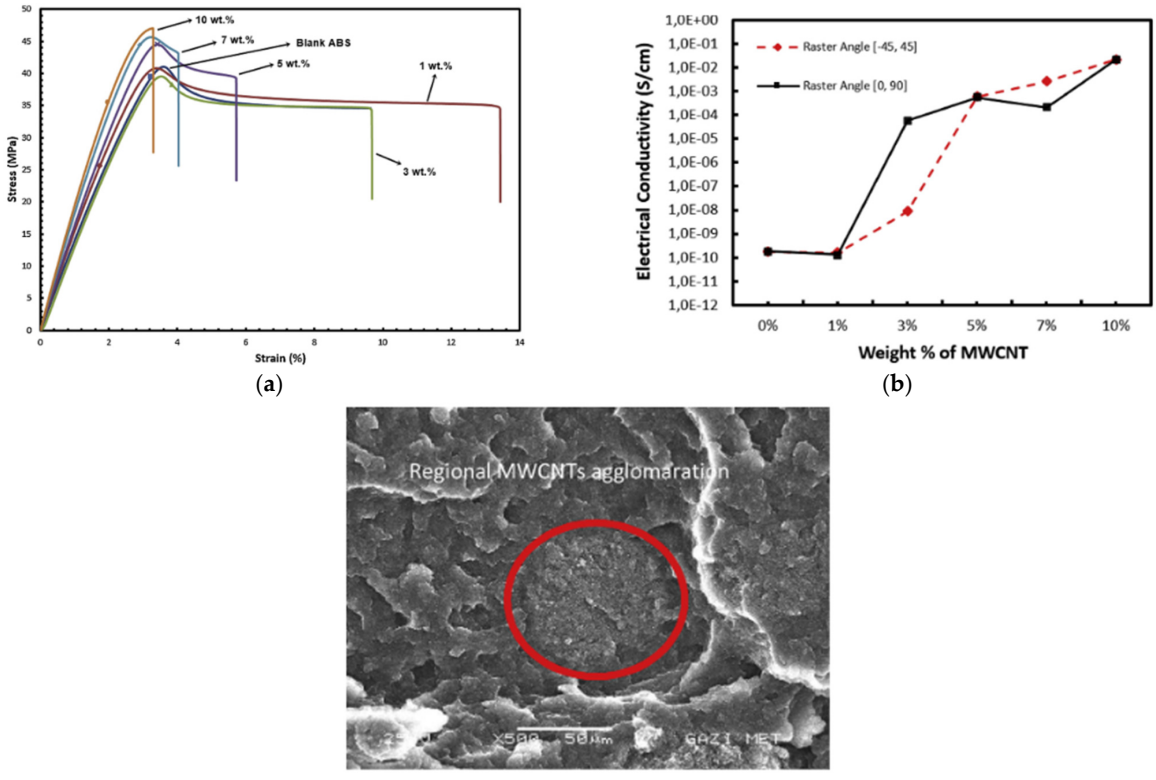

(a) (b)

(c)

Figure 9. (**a**) Stress–strain result of various CNT contents in the polymer matrix. (**b**) Effect of CNTs on the electrical conductivity of printed nanocomposites. (**c**) CNT agglomeration in the nanocomposite [78].

The authors compared the properties of 12 wt% CNT nanocomposite with the injection-moulded parts. The morphology of the filament is shown in Figure 10, demonstrating no voids and spaces, as reported. The mechanical properties, tensile strength, impact resistance, and flexural modulus were 94.45%, 85.51%, and 92.94% of the injection-moulded part. The electrical resistivity was low because the FDM part is less dense than the injection-moulded parts. The wave absorption performance of the FDM part was observed close to the moulded part. The lowest reflection loss, shown in Figure 10b, was lower than the moulded counterpart because of the favourable orientation of the nanotubes in the polymer matrix. Therefore, the FDM method was recommended for such an application.

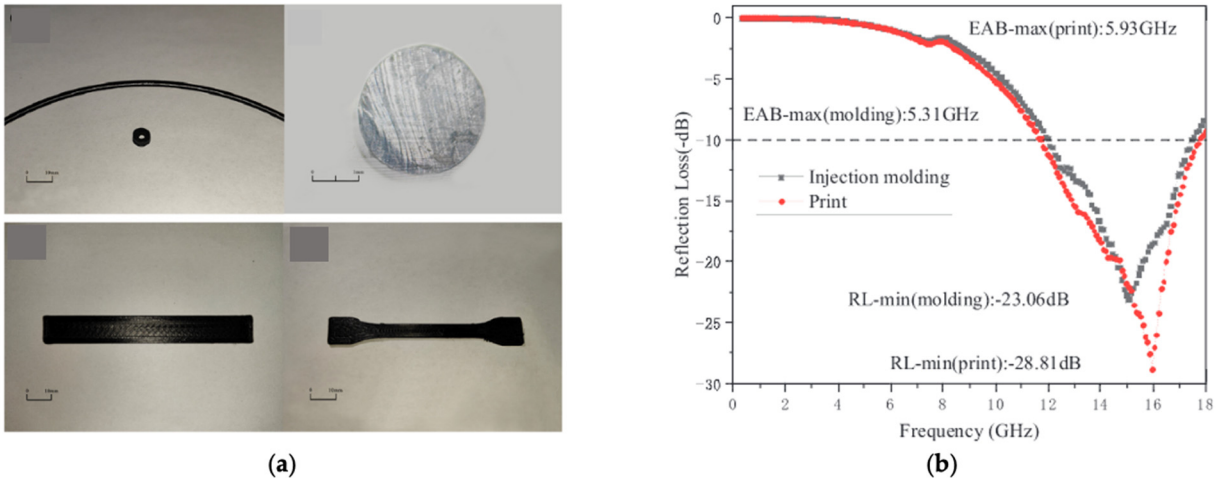

Figure 10. (**a**) CNT-polyamide nanocomposite filament and FDM-printed part. (**b**) Reflection loss performance of the nanocomposite samples [82].

The piezoelectric energy harvester, as an alternate source of energy, was a popular field of research but was dominated by conventional methods [83,84]. Fused deposition modelling has attracted researchers' attention in the alternate energy domain such as energy harvesters. The MWCNT-polyvinylidene fluoride (PVDF)-based piezoelectric energy harvester, having a porous structure [85] and using heat during the printing, was printed. The studied method of foaming was reported to not affect the geometry parts. Figure 11a shows the graphical explanation of the entire process of printing the PVDF-MWCNTs energy harvester. A 1 wt% and 2 wt% nanocomposite's electronic image is shown in Figure 11b, detailing the dispersion of the nanoparticles in the polymer matrix phase. The authors demonstrated that the compressive strength increases from 509.09 kPa to 675.50 kPa for a 2 wt% nanocomposite energy harvester [85]. The dispersed nanoparticles behave as a stress conductor supporting the polymer matrix phase. This induces increased compressive strength. The electrical output, as shown in Figure 11c,d in terms of voltage, increases with the CNT content up to 1% as expected, but with a further increase, it decreases. The reason behind this fall is that the MWCNTs failed to maintain the high aspect ratios in dispersion and became agglomerated. The application of the energy harvester is demonstrated by the running and jumping tests generating up to 25 V and 45 V, respectively.

Biocompatible materials such as FDM-printed nanocomposites have also been investigated. Verma et al. [86] studied CNT-polypropylene random copolymer (PPR) because PPR has a lower glass transition temperature and melting point than polypropylene. This reduces the warping of the part during the printing, making it more ideal as an FDM filament than polypropylene. The authors studied the mechanical performances for 4 wt%, 6 wt%, and 8 wt% of CNT loading. The mechanical performance of the printed parts is shown in Figure 12. For longitudinal loading, the printed parts were strong, with the highest tensile strength and elastic modulus of 8 wt%. A similar trend was observed in transverse-direction loading with a relatively less increase. This was reported to be attributed to the fact that interraster adhesion is weaker in transversion printing than longitudinal. The

piezoresistive response of the nanocomposites was investigated in terms of the gauge factor $(k) = \frac{\Delta R}{\Delta \varepsilon R_0}$, where R_0 is the noload resistance, ΔR is the change in resistance at any load in the composite, and $\Delta\varepsilon$ is the change in the imposed strain. When the mechanical loading is applied to the nanocomposite parts, the distance between the conductive path increases, causing the resistance to change. For low concentrations, this change is high because of fewer conductive paths, but for higher concentrations, the resistivity change decreases because of the high number of conductive path clusters in the PPR matrix.

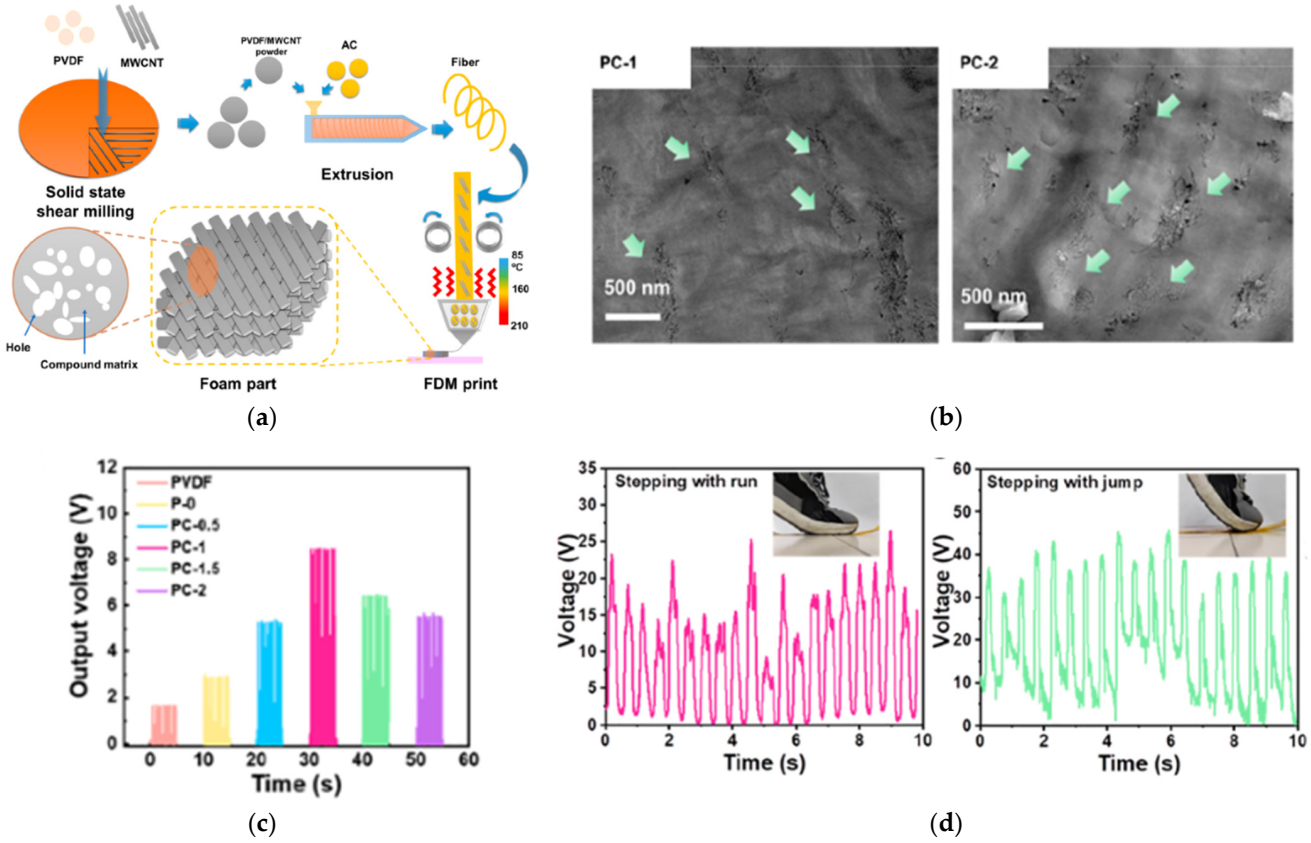

Figure 11. (**a**) CNT-PVDF nanocomposite preparation following the foam printing using FDM. (**b**) Detailed images showing dispersed phases of polymer matrix and CNT. (**c**,**d**) Electrical performance of the energy harvester [85].

Chen et al. [87] studied polyetherimide (PEI) as a polymer matrix with CNTs to improve the bond strength and reduce the porosity in the FDM parts.

The microscopic images show that the dispersion of CNTs in PEI reduces the porosity in the printed parts for all raster orientations. The other advantage reported was the reduction of warping, as shown in Figure 13c, for a 0.6 wt% CNT concentration. The warping in Figure 13a before annealing was improved by up to 40%, and after annealing (b), by up to 46% because the annealing increased the molecular entanglement between different rasters.

Investigations have been carried out for the combination of carbon nanotubes with biocompatible PLA. Petousis et al. [88] used 3D printing of PLA/CNTs nanocomposites together with the carbon dioxide laser-cutting method. The authors studied this new manufacturing technique for the improved properties of printed parts. Kotsilkova et al. [89] reported a rheological study of PLA/CNTs nanocomposites. Yang et al. [90] reported that a 4% CNT addition to PLA improves the electromagnetic shielding properties of the 3D-printed nanocomposites. The authors also reported that by keeping the concentration constant, the properties can be tailored further by altering the process parameters of the FDM process. Shi et al. [46] studied the CNT-PLA nanocomposites experimentally using a local enrichment

method. The method involved depositing a thin layer of nanotubes over the PLA filament, making a locally enriched (LES-PLA/CNT) nanocomposite filament. This is a completely different process than those discussed here, which involves the bulk dispersion of nanotubes and can be termed R-PLACNT nanocomposites. The author compared the printed parts from the filaments prepared using both methods and reported that the LES-PLA/CNT is more electrically conductive than the R-PLA/CNT, as shown in Figure 14. The method offers the huge advantage of saving lots of incurred costs and time in the preparation of bulk dispersed nanocomposites. This method could be used in future research and must be explored for further applications by characterising it for more properties, such as mechanical or tribological ones. Antibacterial properties are very important for any material for biomedical applications. PLA is a biocompatible polymer that was studied by Yang et al. [90] as an MWCNT nanocomposite. Yang et al. [91] showed that the addition of 6 wt% of CNT in PLA resulted in a 64.12% and 29.29% increase in tensile and flexural strength of the FDM-printed part, as shown in Figure 15. The higher layer thickness was suggested to be selected for printing to achieve better improved electrical properties.

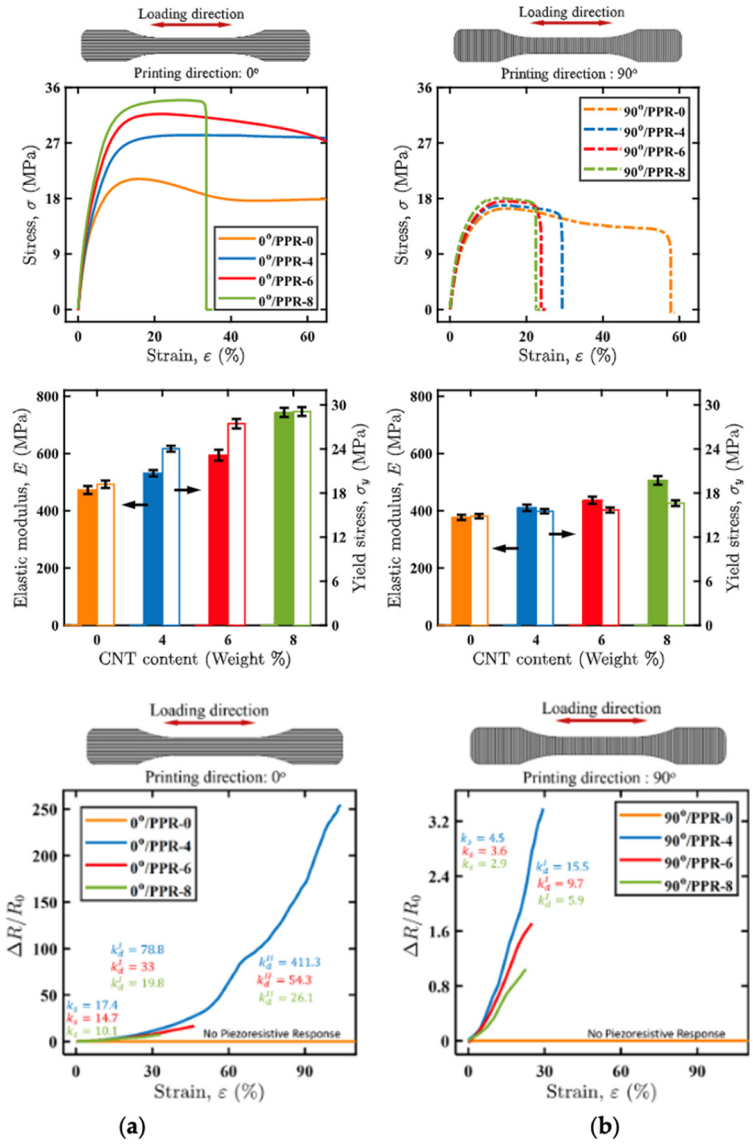

Figure 12. Mechanical and electrical performances of the PPR-CNT FDM-printed nanocomposites are shown for 0° (**a**) and 90° orientations (**b**) [86].

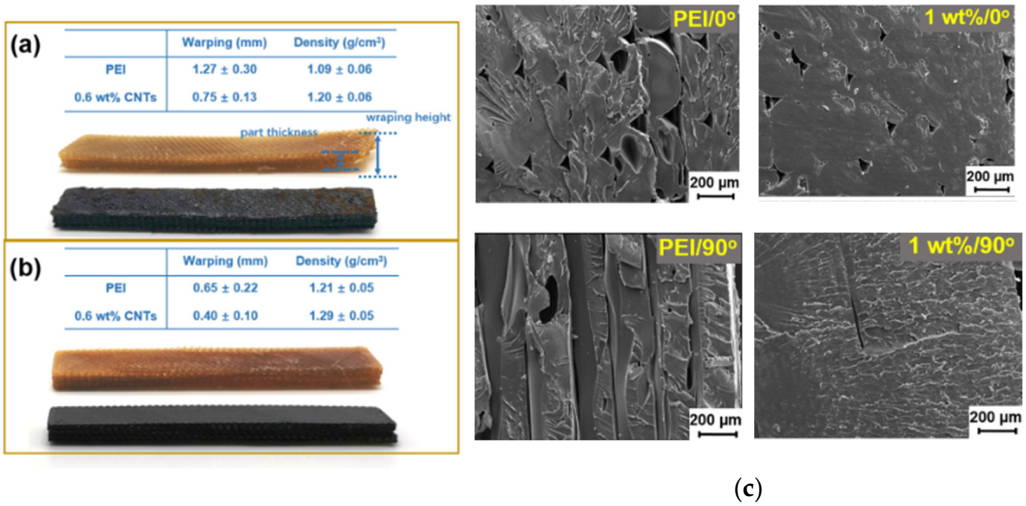

Figure 13. (**a**,**b**) The warping phenomenon in nanocomposite compared to the PEI without. (**c**) Filler's microscopic images of the PEI-CNT showing the voids in the samples [87].

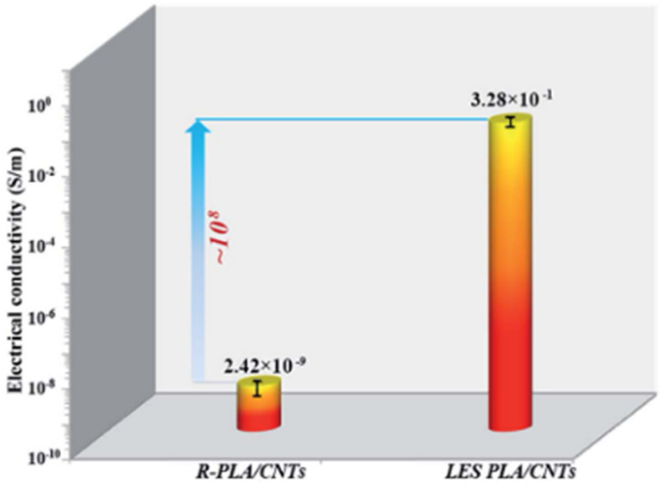

Figure 14. Comparison of electrical conductivity between R-PLA and LES PLA nanocomposites [46].

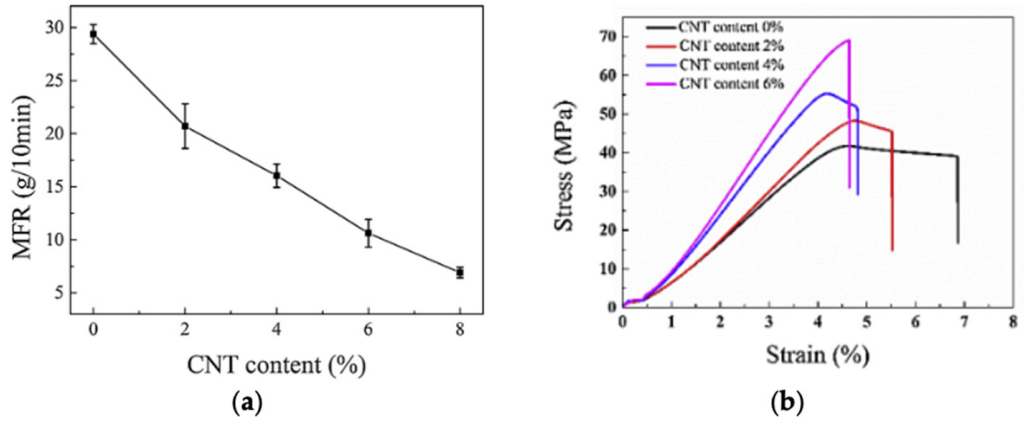

Figure 15. (**a**) Melt flow rate varying with increased CNT content demonstrates the inverse effect of nanofillers in polymer matrix together with (**b**) stress–strain performance of the FDM part [91].

Bortoli et al. [92] reported that the CNT-PLA nanocomposites could demonstrate improved mechanical and other properties at low CNT concentrations when CNTs are functionalised. CNT coils, when dispersed in the polymer matrix, were reviewed. This causes poor stress conduction and, hence, detrimental mechanical performance. For improving

the PLA-CNT nanocomposite performance, functionalised carbon nanotubes (f-CNT) were used as nanoparticles with a PLA matrix instead of commercial CNTs (c-CNT). The authors used nitric acid to create a functionalised group of CNTs. The effect of this oxidisation of CNTs was studied by Raman spectroscopy, as shown in Figure 16a. The $\frac{I_D}{I_G}$ value is defined as the measure of more sp_3 carbon caused by the increased defects on CNTs due to the addition of an oxygen group after functionalization. The $\frac{I_D}{I_G}$ value for f-CNT and c-CNT was reported as 0.64 and 0.49, demonstrating increased sp_3 carbon. The effect of oxidisation was also investigated by differential scanning calorimetry (DSC) analysis. Figure 16b,c shows the first and second heating DSC scans for pure PLA, c-CNT/PLA, and f-CNT/PLA. It was observed that during the first scan, no crystallisation peaks were identified for pure PLA, but for f-CNT, crystallisation peaks were demonstrated to make it a better nucleating agent. In the second DSC scan, the authors reported an increase in T_g from 62 °C (pure PLA, c-CNT) to 65 °C (f-CNT). This could be because the attached oxygen groups might restrict the movement of PLA chains in the f-CNT/PLA nanocomposite.

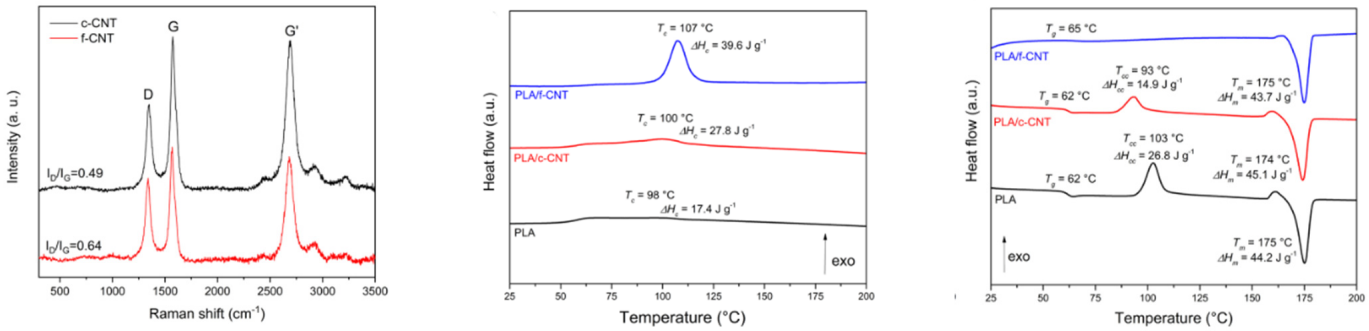

Figure 16. (**a**) Raman spectra of the c-CNT and f-CNT. (**b**,**c**) First cooling and second heating DSC scans of the PLA-CNTs nanocomposites [92].

Upon comparing the performance of the ABS and PLA as a polymer matrix, a similar effect of CNTs was observed in the reviewed literature. This leads to a conclusion that in general, CNTs have the following: (i) A decreasing effect of mechanical properties for lower concentrations because of agglomeration. (ii) There is an increase in elastic modulus and strength beyond the mechanical threshold because of more entangled CNTs increasing the surface area of the matrix. (iii) The electrical properties show an increase beyond the percolation threshold because of the more complete conductive path. (iv) The electrical properties in CNT-filled nanocomposites are because of the tunnelling effect and are of an NTC nature, becoming affected by the heat. Strain sensors need high stretchability together with better electrical properties. The conventional polymers used in FDM, such as PLA, ABS, polyamide, etc., are not suitable because of their linear elastic behaviour [93]. Scientists have reported using polyurethanes (TPUs) because of their low elastic modulus and high strain. Walin et al. [94] reviewed the printing of elastic materials with AM methods and reported that the TPU is the best candidate for FDM as compared to other soft materials such as silicone and hydrogels. It is demonstrated that the TPU can provide about 400% ultimate elongation in the FDM method.

Tzounis et al. [95] characterised the thermoelectric TPU-MWCNT-based nanocomposites. The authors successfully prepared the nanocomposite filaments, printed them using FDM, and characterised them mechanically. It was reported that out of 1.0%, 2.5%, and 5.0%, the last showed the highest tensile modulus. The study utilised two different types of CNTs, commercially available NC-MWCNTs, and long-diameter LC-MWCNTs, both exhibiting different properties. The morphological study, as shown in Figure 17, revealed that the dispersion was homogeneous. The LC-MWCNT-printed samples demonstrated high roughness at the fracture surface in comparison to the others because of the longer nanotubes. The study reported that for 5% TPU-MWCNTs, the samples could be strained

up to 110% and 129%, as shown in Figure 17. The reason attributed could be because of either CNT's small micro agglomeration acting as a stress concentration or the poor interlayer bonding between the layers of the printed parts.

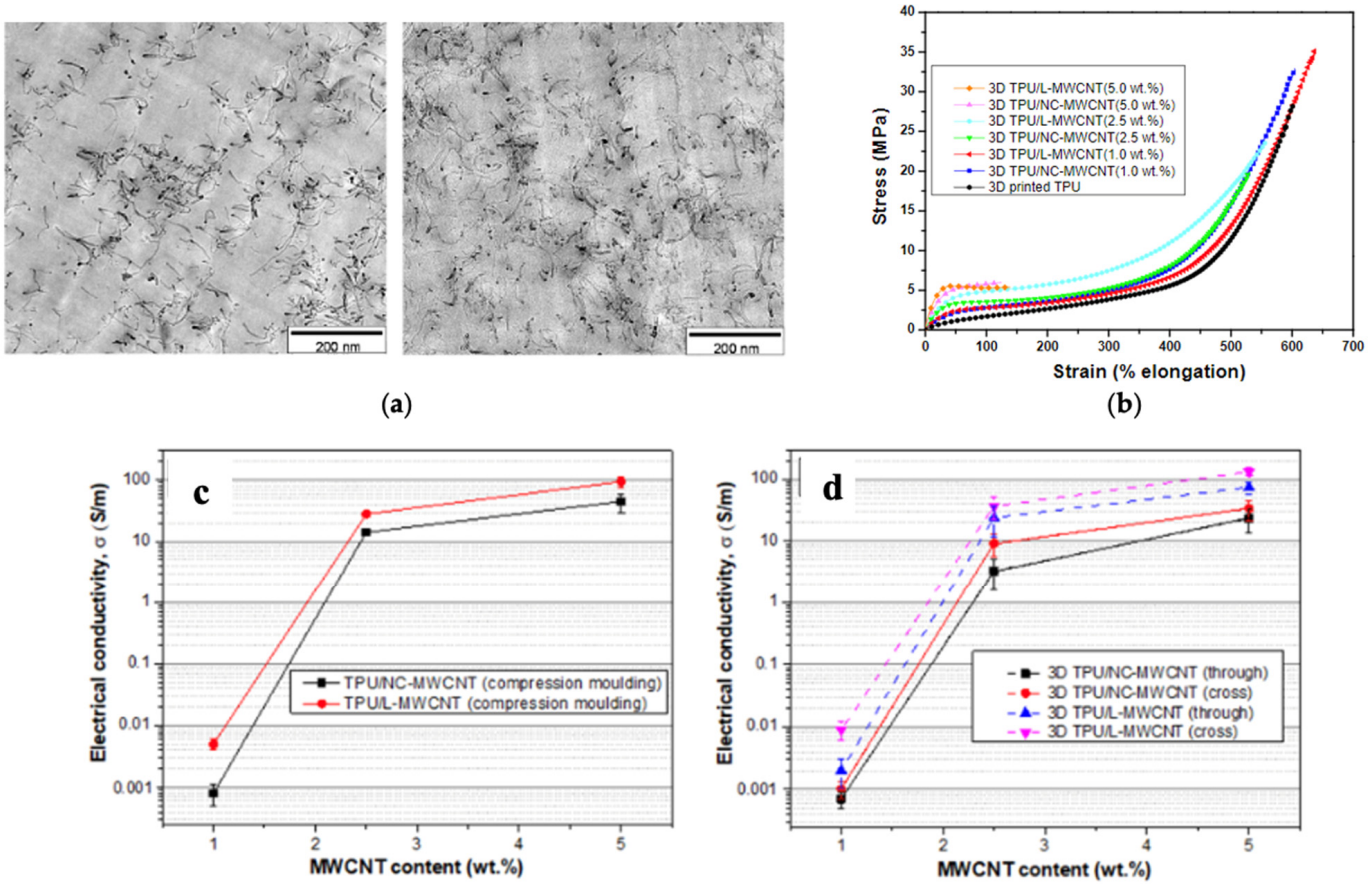

Figure 17. (**a**) Morphology showing the dispersion of CNTs in the TPU matrix. (**b**) Mechanical performance of the TPU-CNT composite. (**c**,**d**) Effect of CNTs on the electrical conductivity of the MWCNT-TPU nanocomposites [95].

The printed parts reported anisotropic behaviour in electrical conductivity. The cross-layer conductivity is higher in comparison to along the layers because of the more oriented CNTs during the printing in that direction, as interpreted by the authors. Li et al. [96] proposed a novel method to develop TPU-CNTs auxetic nanocomposite structures. The authors printed the structures using the FDM method, subsequently coating them with CNTs in an ultrasonic bath, as shown in Figure 18.

The nanocomposite auxetic structures demonstrated a 0.8 Poisson's ratio with a 300% strain, as shown in Figure 18. The deformed morphology is shown in Figure 18c for different CNT concentrations. Recently, many other matrix compositions have started to attract scientists' attention. Studies have been reported for combinations such as TPU/PLA/CNTs [97], biobased TPU [98], and ABS-PBT-CNT [99]. Table 1 summarises the latest polymer nanocomposites studied using the FDM method.

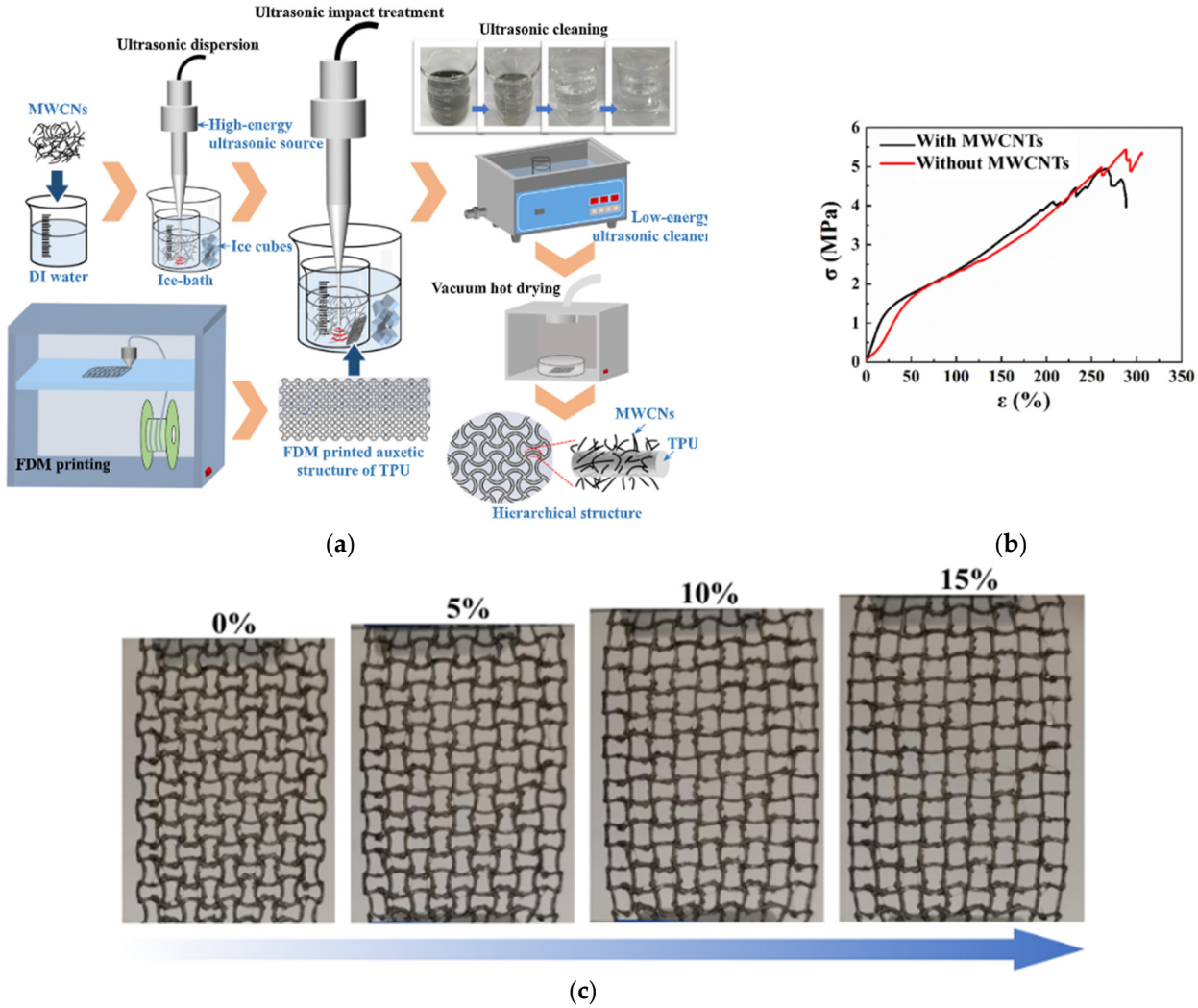

Figure 18. (**a**) Schematic representation of the prepared auxetic nanocomposites printed via FDM. (**b**) Effect of nanofillers on the mechanical performance of the structures. (**c**) The stretchability of the FDM nanocomposite auxetic structures [96].

3.2. Graphene Polymer Nanocomposites

A single sheet of graphite with only two dimensions as graphene has reported excellent mechanical and electrical properties [100]. To improve the final performance of FDM polymers, scientists have doped these polymers to print nanocomposites with improved properties [42,101–104]. Gananasekaran et al. [64] prepared CNT/graphene-based polybutylene terephthalate (PBT) nanocomposite and compared the CNT-PBT and graphene-PBT nanocomposites. The study revealed that the CNT-based nanocomposites demonstrated better mechanical properties than graphene-based ones. The CNT-PBT filament was less brittle than the graphene-PBT filament. The reason attributed to such behaviour was during the evaporation, the moisture associated with graphene sheets creates voids in the printed part. The electrical percolation threshold for CNT-PBT and graphene-PBT was reported to be a minimum of 0.49 wt% and 5.2 wt%, respectively, to make the FDM-printed parts conductive. One challenge faced by researchers in printing such nanocomposite is the abrasive nature of nanoparticles in the matrix. Figure 19 shows the nozzle before printing (a), printing 10 cm of PBT-graphene (b), and 1.5 m of CNT-PBT nanocomposite (c) along with the electronic image of the graphene-PBT printed via an abrasive nozzle (d). The effect can be seen through the images and could be interpreted that CNT-based nanocomposites tend to erode the nozzle relatively higher than those that are graphene-based.

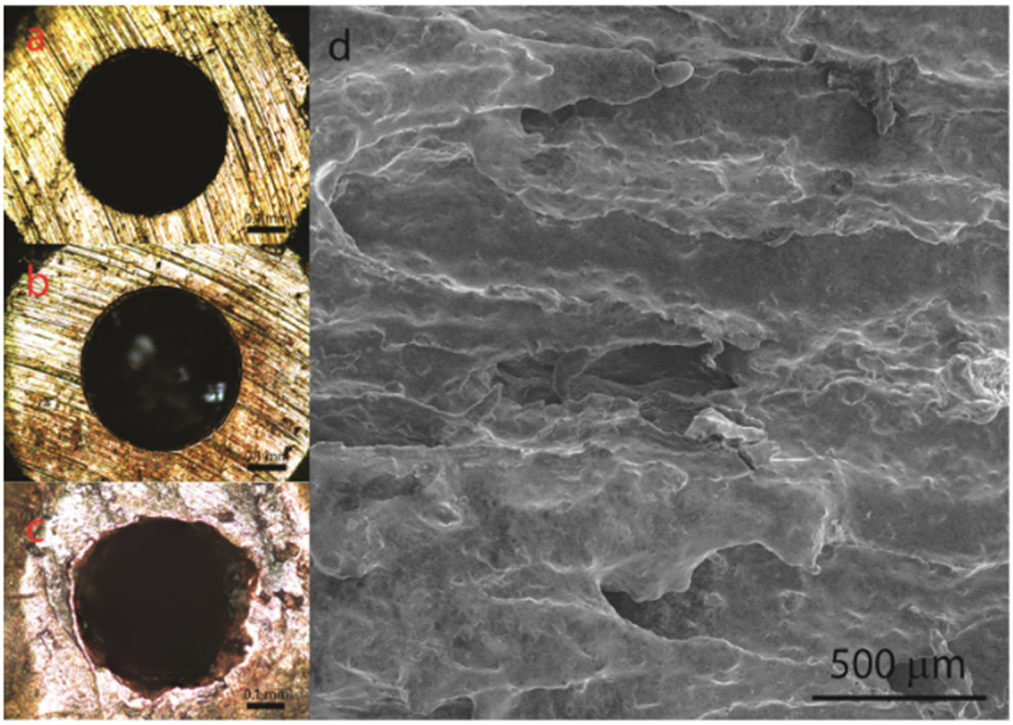

Figure 19. Erosion effect of graphene on the nozzle of FDM printer and the microscopic image of nanocomposite (**a**), printing 10 cm of PBT-graphene (**b**), and 1.5 m of CNT-PBT nanocomposite (**c**), along with the electronic image of graphene-PBT printed via an abrasive nozzle (**d**) [64].

Camargo et al. [105] printed commercially available graphene and ABS nanocomposites and characterised them for their mechanical and electrical properties. The authors reported that the addition of graphene deteriorates the tensile strength of the nanocomposites opposite to PLA-graphene. The study reported a decrease of 104.6% in yield point. A similar decrease is demonstrated in the flexural strength of the printed nanocomposites in the three-point bending test, 94.6% less than ABS. The impact energy of the pure ABS printed parts was 58.5% greater than the nanocomposites. The reason for this decrease is attributed to the molecular chemistry of the polymer matrix. The butadiene part of the ABS is responsible for high mechanical properties, but the graphene weakens the molecular structure of the rubber part and decreases the final performance. The nanocomposite FDM parts were reported as semiconductors using electrical characterisation.

Graphene nanocomposites printed using FDM have been studied for thermal conductivity. Tambrallimath et al. [106] prepared a dual polymer matrix infused with graphene nanofillers. PC-ABS was mixed in a 70:30 ratio and mixed with 0.2 wt%, 0.4 wt%, 0.6 wt%, and 0.8 wt% graphene. The filaments after printing were characterised using the Maxwell and Bruggeman model. The authors reported an increase of about 15% and 40% in thermal conductivity, as shown in Figure 20, for the 0.2% and 0.8% graphene contents. In the literature, authors have reported that because of the addition of graphene in the polymer matrix, there is a reduction in phonon scattering, hence decreasing the thermal conductivity [107,108]. The study did not provide substantial validation and claims for the findings. In a subsequent study, the same authors extended the investigation, and Figure 21 shows the electron images of the nanocomposites [109]. The images show that the graphene dispersed homogenously without any visible agglomeration.

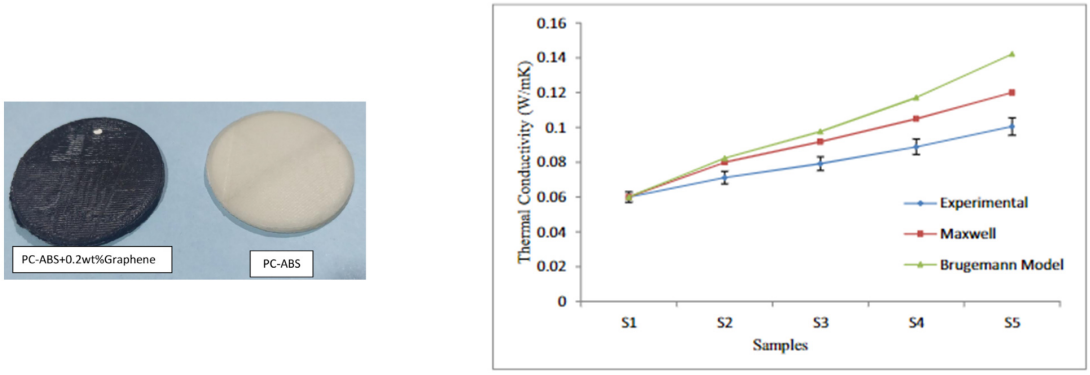

(**a**) (**b**)

Figure 20. (**a**) PC-ABS-graphene double-polymer matrix nanocomposite. (**b**) Thermal performance of the double-matrix nanocomposite [106].

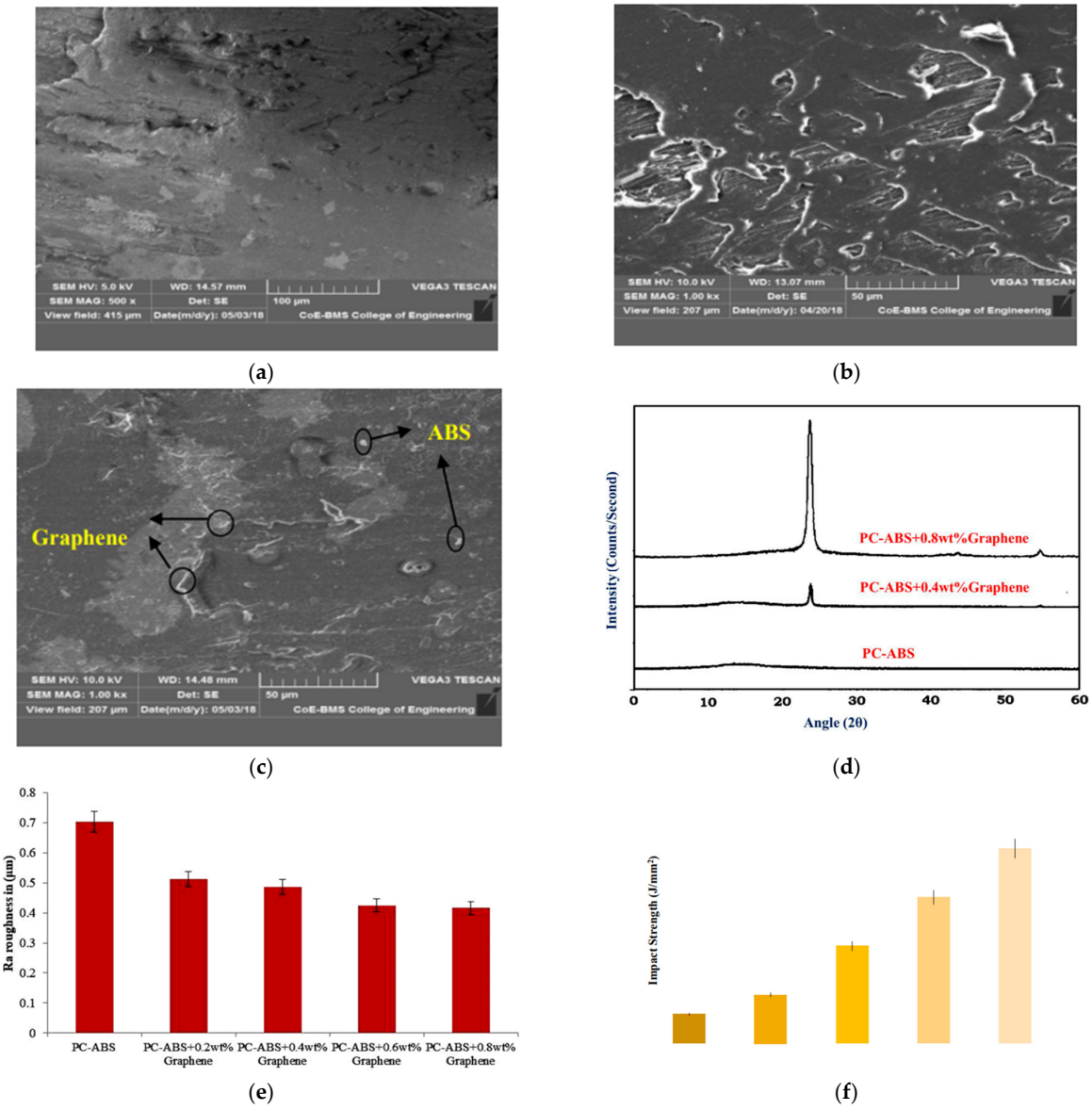

(**c**) (**d**)

(**e**) (**f**)

Figure 21. (**a**) PC-ABS, (**b**) PC-ABS-0.4% graphene, (**c**) PC-ABS-0.8% graphene, and (**d**) XRD spectra of the (**a**–**c**) samples. (**e**) Surface roughness characterisation and (**f**) impact performance of the nanocomposite samples [109].

It should be taken that upon increasing the graphene content, it tends to agglomerate because of the presence of van der Walls forces. The mono-layer graphene exhibits better properties because of the warping, crumpling, or folding [110]. The presence of graphene is characterised by the X-ray diffraction (XRD) method. Figure 21d shows the XRD results for the graphene nanocomposites; the sharp peaks in the curve indicate the presence of graphene, and the intensity increases with the content of graphene. The authors analysed the surface roughness of the nanocomposites and reported that with an increase in graphene content, the surface finish increases. A maximum of 40% reduction in surface roughness was reported for the 0.8% graphene content, as shown in Figure 21e. The reason for increasing the impact strength upon the graphene addition is that the nanofiller inhibits the deformation in the polymer matrix along with fewer voids in part. The functional group attached to graphene, such as oxygen, enhances the properties of the nanocomposites. The additional functional group increases the interfacial interaction with the polymer matrix. This motivated the researchers to investigate the effect of reduced graphene oxide (r-GO) in polymer matrix nanocomposites printed using FDM [111]. There are few studies available with graphene as nanofillers in the FDM method. Challenges remain the same because, at higher nanofillers, proper dispersion without agglomeration becomes difficult. Also, the other matrices, such as PC, PLA, PEEK, etc., could be explored for many other applications.

For the FDM method, the viscosity of the melt is a very important feature. The viscosity must not be high for the polymer melt to flow out of the nozzle easily and should not be low to maintain the structural integrity once placed as a layer. Therefore, the addition of nanofillers, such as CNTs and graphene, induces a large degree of orientation among polymer chains during the shearing, and this reduces the viscosity with a better flow out of the nozzle. Once out of the nozzle, the shear reduces abruptly, increasing the viscosity of the melt [112–114]. Shmueli et al. [115] investigated this effect in isotactic polypropylene graphene nanoplatelet nanocomposites using the in situ FDM process. The authors studied the 5 wt% and 10 wt% graphene contents and reported that graphene induces shear thinning in FDM nanocomposites. The in situ analysis revealed that the graphene polymer produces a weak lamellar structure, causing a decrease in storage modulus in 5% graphene content. This structure vanishes when the graphene is increased up to 10%, leading to an increase in thermal conductivity.

Shi et al. [45] printed a hybrid PLA/CNTs/graphene nanocomposite cellular structure for an electromagnetic interference (EMI) shielding application. The authors prepared the filament by producing a coating of CNT/graphene nanofillers over PLA particles. These filaments, upon characterisation, demonstrated that the CNT/graphene fillers were attached effectively to the matrix because of the hydrogen bonding physical interactions. These interactions were increased because of the intersected CNTs, together broadening the contact areas for stronger matrix filler interactions. To understand the behaviour of polymer melt in the FDM process, authors have characterised the fluid melt behaviour using finite element simulation (FES), as shown in Figure 22. It was observed that the shear rate distribution was uniform in the channel. Figure 22(a1) represents equally spaced streamlines on the half Y–Z planes in the +Z direction. The steady shear rate in the lower range of 100–103 s^{-1} was observed at the start, leading to a maximum shear rate of 808 s^{-1} at the convergence channel. There was no turbulence observed, and the steady flow demonstrated the suitability of the prepared nanocomposite for the FDM process. Figure 22d to e represents the printed nanocomposite samples and the SEM image of the top layer showing the proper dispersion of the nanofillers. The effect of these nanofillers can be seen in Figure 22f,g in the stress–strain curve and tensile strength, respectively. The SEM images shown in Figure 22h after the fracture provide evidence of low deformation in the nanocomposite (h2) in comparison to PLA (h1). Jing et al. [50] investigated the thermal conductive nature of polyethylene graphene nanocomposites. The authors reported increased thermal through-plane conductivity (~3.43 W m^{-1} K^{-1}) along the printing. The attributed reason was due to the reduction in interfacial thermal

resistance along with the long-range connected network of graphene with the polymer matrix [50].

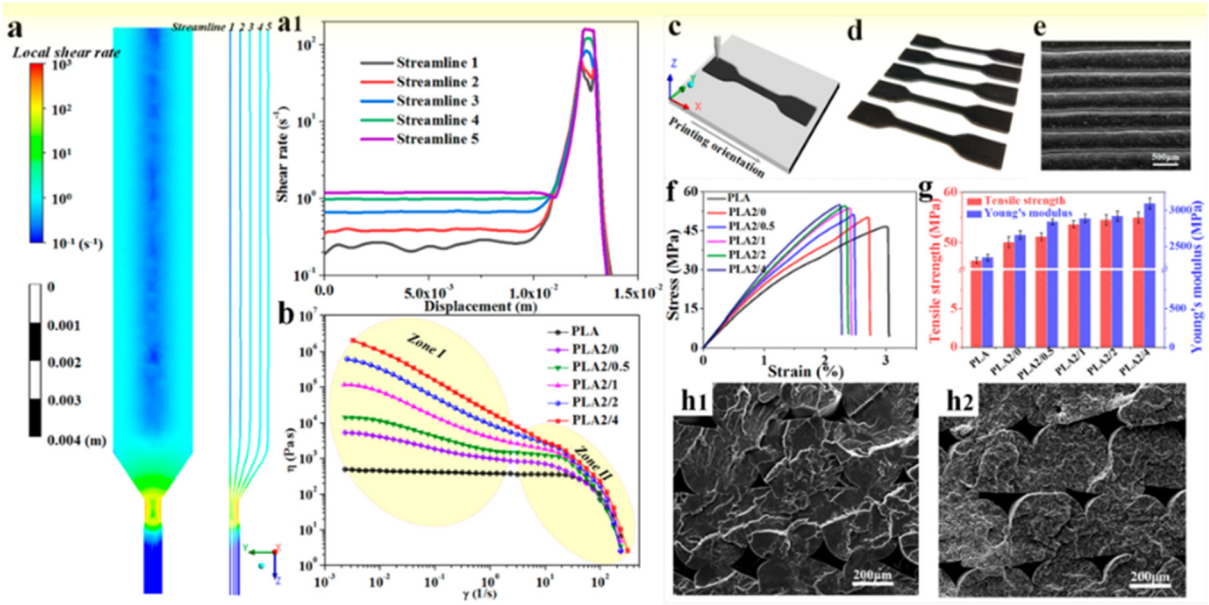

Figure 22. (**a**) Shear rate distribution for the polymer melts on the full channel. (**a1**) The shear rate curves on the half of Y–Z planes in the +Z direction. (**b**) Apparent viscosity of polymer and polymer nanocomposites as a function of shear rate. (**c**,**d**) Schematic diagram of standard FDM samples. (**e**) The corresponding microscopic image of the top surface of the printed samples. (**f**,**g**) Stress–strain performance of the FDM 3D-printed samples and tensile strength. (**h**) Microscopic images of the fractured samples of PLA (**h1**) and PLA2/2 (**h2**) samples [45].

The hybridisation of nanocomposites has been studied by combining two different types of nanofillers. Ivanov et al. [116] studied the commercially available graphene and CNTs in a PLA polymer matrix. The authors investigated the individual nanofibers in a PPLA matrix together with the hybrid graphene/CNTs in PLA. The confirmation of walls in nanotubes and sheets in graphene is characterised by Raman spectroscopy. The spectrum of graphene, as shown in the Figure, is characterised by the G, D, and 2D bands (peaks). The G signifies the in-plane vibrational mode because of the sp_2 carbon atoms. The G-band shift towards a higher wavenumber in the spectrum marks the presence of a low number of sheets in graphene. The defects in the lattice of graphene-carbon are associated with the D band. The intensity ratios (I_D/I_G) and (I_{2D}/I_G) give an insight into the quality of graphene and the structural disorder degree—a ratio of 2 signifies defect-free graphene. If the spectrum presents a sharp single 2D peak, it is a confirmation of single-layer graphene. For multilayer graphene, this band splits into multiple bands [117,118]. The spectra of 6 wt% and 1.5 wt% graphene nanocomposites show a D band at 148 cm^{-1} and 1356 cm^{-1}, respectively, signifying the decreased defects with increased graphene content due to heating and shearing damage in extrusion. For the MWCNT nanocomposites, the D and 2D bands provide information regarding the presence of a disordered carbon lattice and the effect on the vibrational modes due to nanotube–nanotube interactions [119,120]. The figure shows broad D and 2D bands, signifying large diameters, high disorders, and a high number of walls in the nanotubes. The sharpness and intense G bands are demarcations of better dispersion of CNTs in the polymer matrix [121], which is indicated by Figure 23 for the PLA/MWCNTs nanocomposites. The literature presents many polymer matrices in combination with graphene or reduced graphene nanoparticles, but in comparison to the CNTs, there is still more polymer matrix that needs to be studied to expand industrial acceptance.

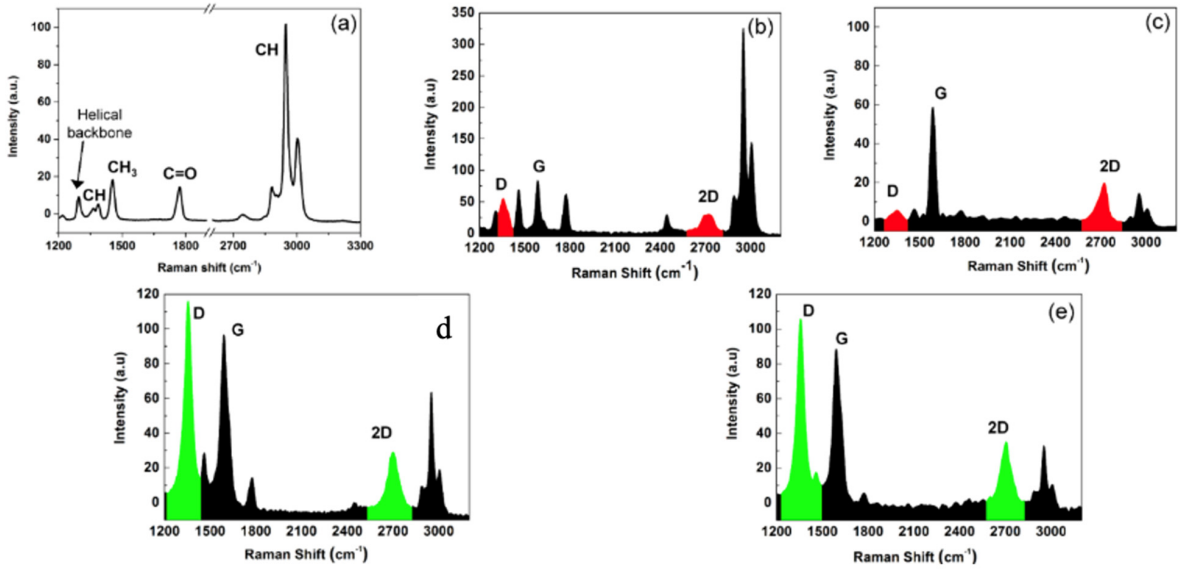

Figure 23. Raman spectra of pure PLA (**a**), graphene-PLA (**b**,**c**), and CNT-PLA (**d**,**e**) [116].

3.3. Cellulose Polymer Nanocomposites

PLA has been a popular choice for biocompatible polymers besides others, such as WBPUU or WBPU [122–124]. Researchers have been using biocompatible nanofillers to enhance the properties of the filament and the final printed parts, together with biocompatibility. Cellulose nanocrystals (CNCs) were reported to improve the thermal and mechanical properties when dispersed in a PLA matrix [125–128]. The reason for this is that the CNC acts as a crystallising nucleating agent. Therefore, upon loading the nanocomposites, the oriented CNCs in polymer absorb the load, improving the tensile strength of the part [129,130]. The CNCs demonstrate low weight, transparency, biocompatibility, and strength [131,132]. The CNC exhibit 54–88% of crystallinity, which is the reason for its high tensile modulus (105–250) GPa, greater than steel wire and glass fibre [133,134]. But, CNC's crystallinity acts as a nucleating agent when dispersed into the PLA matrix, affecting the final mechanical properties of the nanocomposites (Figure 24).

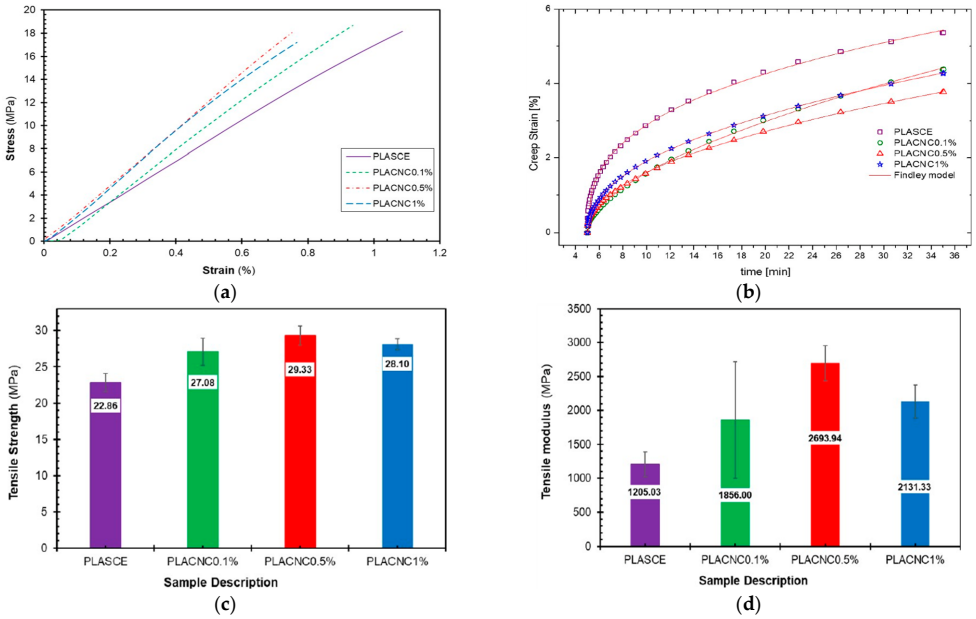

Figure 24. Mechanical characterisation results of PLA-CNC nanocomposites ((**a**) stress–strain, (**b**) creep, (**c**) tensile strength, and (**d**) tensile modulus) [135].

Wu et al. [136] studied PLA/CNC nanocomposite, focussed on the homogeneous dispersion of CNCs using the melt-bled method in comparison to the solution method. The authors used polyvinyl acetate (PVAc) to graft with CNC which later compounded with PLA matrix exhibited excellent dispersion. The prepared 5 wt% nanocomposites demonstrated increased melt processibility and interlayer adhesion of filament, finally increasing the tensile break energy (254%), notched impact toughness (57%), and interlayer adhesion (103%). Kusmono et al. [137] reported the effect of nanocrystalline cellulose (NCC) on a neat PLA matrix. The NCCs were extracted from ramie fibres using chemical treatment via sulphuric acid and hydrolysis. The prepared NCC power was mixed with PLA and extruded at 185 °C for 1, 3, and 5 wt%. The authors reported that 1 wt% NCC into the PLA matrix increased the tensile strength by 19.04%. The further increase in concentration deteriorated the mechanical strength of the nanocomposite, which was attributed to an increased agglomeration of nanofillers in the matrix. Agbakoba et al. [135] extracted the CNC from Eucalyptus sawdust using chemical means, which were blended with PLA. The increased flexural strength in the three-point bending test, as shown in Figure 24, is because of the crystallinity of CNC, but due to agglomeration at 1 wt%, there is a slight decrease. The creep behaviour was studied at 35 °C; all specimens showed similar primary creep behaviour, but the nanocomposites demonstrated lowered secondary creep deformation, as shown in Figure 24. This is indicative of a high modulus, which is shown in the results of three-point bending tests. The attributed decrease in tensile modulus and strength is because of the agglomeration of CNC when increased at 1 wt%. It is very evident from the reviewed literature that the hydrophilic nature of CNC and high crystallinity, together with poor dispersion into the polymer matrix PLA, need to be challenged. Wu et al. [138] incorporated TPU droplets at the nanoscale into the PVAc-treated CNC into the PLA polymer matrix to improve the melt processibility of nanocomposites. The authors reported an increase of 418% ductility at 5 wt%. This is a remarkable improvement in comparison to others, which reported a decrease in the mechanical properties when CNC is increased beyond 1 wt% due to agglomeration.

Other forms of cellulose, such as cellulose nanowhiskers (CNW), are more compatible with PLA because of the hydroxyl group due to silylation [139]. Cellulose nanofibres (CNF), another nanofiller class of cellulose, have attracted researchers for study. High-density polyethylene (HDPE) is a challenge to print using FDM because of its high warping and massive shrinkage properties. Therefore, to increase the printability, Dalloul et al. [140] studied chemically modified CNFs as nanofillers in the HDPE matrix. The CNFs, before the mix, were treated with an esterification reaction, converting them to polystearyl acrylate-grafted CNFs. The resulting nanocomposites were characterised experimentally and were reported with improved mechanical properties. For a 10 wt%, an increase of 23% in Young's modulus was reported with no CNF agglomeration. However, it is to be noted that the authors reported a decrease in the tensile strength of the nanocomposite samples; Figure 25. The reason was the FDM nanocomposites had increased stiffness because of the filler processing, and this reasoning has been attributed to other works as well [141,142].

The flexible polymer matrix polyurethanes have been a popular choice for FDM printing because of their flexibility. These polymers consist of a hard segment formed by isocyanate, a chain extender, and a soft segment of polyol. The rigidity is provided by the hard segment, and the soft is responsible for the flexibility of the polymer, thus varying the precursors while synthesis provides myriad properties in such materials [143,144]. However, to produce more environmentally friendly and biocompatible polyurethanes, such as waterborne polyurethanes (WBPU) and ureas (WBPUU), they have been studied for FDM printing materials. The issue with these materials is that because of their high flexibility, the filament demonstrates entanglements in gears and Bowden extruders due to high friction [145,146]. Therefore, to enhance printability, researchers are focussing on using nanofillers as a solution.

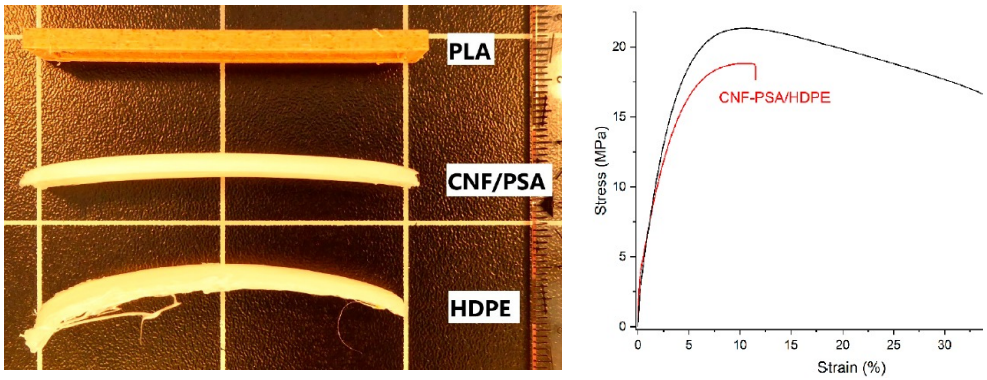

(**a**) (**b**)

Figure 25. (**a**) Improved warping characteristic of HDFE due to esterified CNF nanofillers. (**b**) Stress–strain graph showing the decreased tensile strength due to nanofiller [140].

Larraza et al. [147] synthesised the WBPUU polymer and prepared graphene/WBPUU nanocomposites. The biocompatibility of the polymer is tested via cytotoxicity, as shown in Figure 26. The minimum short-term cell viability negative value, as per the ISO 10993-5 standard, is less than 20 for 24, 48, and 72 h. The prepared polymer demonstrated 70% higher values in all cases, signifying the non-toxic nature of the polymer. Furthermore, the study of cells was conducted via cell proliferation and adhesion investigation, as shown in Figure 26b. The authors reported that the samples had high cellular density with very few dead cells. The viable cells showed increased density after a week of study, demonstrating the high compatibility of the polymer as a biomaterial. The nanocomposites were reported to have improved printability and mechanical properties upon characterisation.

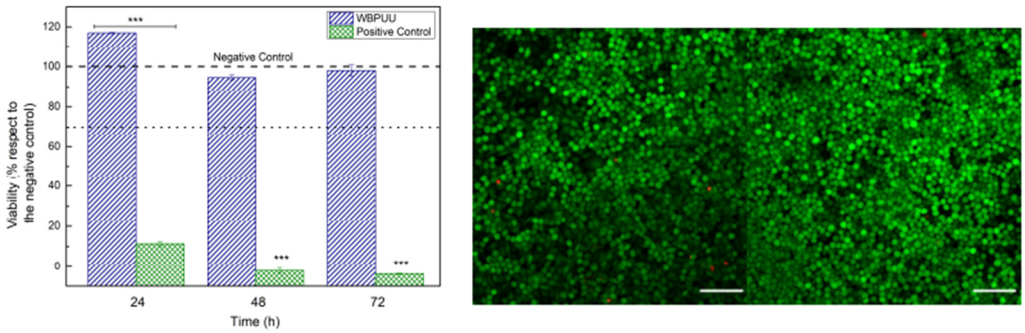

(**a**) (**b**)

Figure 26. (**a**) Viability result of L929 murine fibroblast cells on the polymer concerning time. (**b**) Adhesion and viability of L929 cells for 3 and 7 days (left and right), respectively [147].

Aside from PLA, another polymer matrix in combination with PLA has been studied. Frone et al. [148] prepared cellulose fibres with lignin (CFw), without lignin (CF), and plasticised poly (3-hydroxybutyrate) (PHB) on the properties of PLA. The incorporation of lignin has the effect of improving the thermal properties of the nanocomposites in comparison to those without lignin. Wang et al. [43] showed that the thermal stability and mechanical properties (tensile strength and elongation at break) can be improved by using CNF in PLA. For smart applications and self-healing, a nanocomposite with a polymer matrix of TPU and polycaprolactone (PCL) with CNC was investigated by Bi et al. [149] via the solution casting method and was used to prepare the nanocomposites. The tensile testing of these samples reported an increase in interfacial adhesion because of more crosslinking due to CNC. Further, 1 wt% CNC increases the strain up to 1600%. Without CNC, the dispersibility of PCL in TPU was poor. Upon addition of CNC, the PCL agglomerates decrease in the TPU phase for 0.5 wt% and 1 wt% compared to TPU-PCL without CNC. The cellulose-based nanofillers present many filler types, as reviewed, and

many more. The important aspect of these fillers is that they are completely biocompatible, and the nanocomposites with biobased polymer matrix, such as water-based polyurethane or PLA, create improved FDM parts with superior biocompatibility. This opens doors for researchers to investigate the possibility of industrial acceptance of such nanocomposites for biomedical applications.

Table 1. Different polymer matrix nanofiller filament preparations.

Matrix	Method	Properties	Ref.
ABS + CNT	Chemical solution	Electrical and mechanical properties, mechanical percolation threshold (9%), electrical threshold percolation (4.76%)	[48]
ABS + CNT	Mechanical (melt mixing)	Rheological, morphological, and mechanical properties, 2% CNT increases strength by 42%	[68]
ABS + CNT	Mechanical (melt mixing)	Thermal, electrical, and mechanical properties for SWCNTs and MWCNTs	[49]
ABS + Graphene	Mechanical (melt mixing)	Recycled ABS-graphene for rheological, thermal, magnetometric, and mechanical properties	[150]
ABS + Reduced graphene oxide (rGO)	Chemical solution	Interface stresses	[111]
PC-ABS + Graphene	Mechanical (melt mixing)	Tensile strength, low-velocity impact strength, and surface roughness	[109]
PC-ABS + Graphene	Mechanical (melt mixing)	Thermal conductivity	[106]
ABS + Graphene/CNTs	Mechanical (melt mixing)	Stiffness, creep stability processability, tensile strength, and electrical properties	[52]
Polybutylene terephthalate (PBT) + Graphene/CNTs	Chemical solution	Printability, electrical conductivity, and mechanical stability	[64]
ABS + Graphene	Mechanical (melt mixing)	Mechanical (tensile, flexural, and impact) and electrical properties	[105]
Polyethylene + Graphene	Mechanical (melt mixing)	Thermal conductivity and mechanical properties	[50]
Polyurethane + Cellulose/graphene	Chemical solution	Morphological, thermal, mechanical, and thermoelectric properties	[95,147]
PLA + CNTs/graphene	Mechanical (melt mixing)	Electrical and thermal properties	[116]
PLA + CNTs/graphene	Chemical solution	Electromagnetic shielding	[45]
Polypropylene + Graphene	Mechanical (melt mixing)	X-ray scattering and shear study	[115]
ABS + CNTs	Mechanical (melt mixing)	Morphological, electrical, and mechanical properties	[67]
Polyamide + CNTs	Chemical solution/mechanical	Electromagnetic wave absorption and mechanical properties	[82]
PVDF + CNTs	Mechanical (mixing)	Piezoelectric and mechanical properties for energy harvesting	[83]
Polybutylene Terephthalate (PBT)/ ABS + CNTs	Mechanical (mixing)	Mechanical and morphological properties	[99]
Polypropylene random copolymer (PPR) + CNTs	Mechanical (mixing)	Piezoresistive properties (crystallinity)	[86]
Polyetherimide (PEI) + CNTs	Mechanical (mixing)	Bond strength, porosity of parts, electrical conductivity	[87,151]
PLA + CNTs	Chemical/mechanical (mixing)	Thermal, mechanical (dynamic analysis)	[92]
ABS + CNTs	Mechanical (mixing)	Morphological, thermal, and mechanical properties	[71,78]
ABS + CNTs	Mechanical (mixing)	Structural, morphological, and dynamic mechanical properties	[72]
Polyphenylene sulphide + CNTs	Chemical solution	Tensile, bending, diffusion, and thermal properties	[79]

Table 1. *Cont.*

Matrix	Method	Properties	Ref.
PLA + CNTs	Mechanical (mixing)	Thermal, mechanical, and electrical	[88]
PLA + Graphene/CNTs	Local enrichment	Electrical conductivity, electromagnetic interference shielding	[45,46]
ABS + Carbon nanofibre	Mechanical (mixing)	Tensile, dimensional, surface properties	[152]
PLA/TPU + CNTs	Mechanical (mixing)	Morphological, interfacial, and mechanical properties	[51]
TPU + Conductive carbon	Mechanical (mixing)	Biocompatibility, thermal, mechanical	[153]
TPU + CNTs	Mechanical (mixing)	Warping, interlayer adhesion, thermoelectric properties	[95,98]
PLA + Cellulose nanocrystals (CNC)	Mechanical (mixing)	Shape memory properties, melt processibility, and inter-fuse adhesion	[135,136]
PLA + Cellulose nanofibrils (CNF)	Mechanical (mixing)	Thermal stability, mechanical performance, and water absorption	[43]
PLA + Nanocrystalline cellulose (NCC)	Mechanical (mixing)	Tensile and thermal properties	[137]
TPU/polycaprolactone (PCL) + CNC	Chemical solution	Chemical structure, mechanical, and thermal properties	[149]
Poly(3-hydroxybutyrate) (PHB)/PLA + Cellulose fibres (CF)	Mechanical mixing	Structural, morphological, mechanical	[148]
PLA/TPU + CNC	Mechanical mixing	Melt processibility, shear, and stretching effect	[138]
High-density polyethylene (HDPE) + Cellulose fibres (CF)	Mechanical mixing/chemical solution	Warping, morphological, and mechanical properties	[139]

4. Discussion and Concluding Remarks

The present study details an exhaustive review of the CNT-, graphene-, and cellulose-based polymer nanocomposites for the FDM method. The first step in the fused deposition modelling is the feedstock filament, which must be in a printable form. This is a challenging task when processing nanocomposites because dimensional stability is very difficult to achieve.

All the investigation techniques reviewed were experimental methods. There are very limited computational models or methods for investigating the effects of such nanofillers on the performance of FDM-printed parts. Since the parameters of the FDM method, such as the layer height, raster orientation, infill density, etc., affect the final properties of the part, efficient computational models are necessary to understand how these parameters affect the nanocomposites when printed via the FDM technique. Very few studies have been reported that predicted the elastic properties of graphene polymer nanocomposites. Moola et al. [154] demonstrated the application of a representative volume element (RVE)-based approach for nanocomposite printed parts. The model is dependent on the experimental data for investigating the properties. Another computational study by Rinaldi et al. [155] was based on the Piggot model, the Takayanagi I model, and the Takayanagi II model. The authors applied the respective models to study PEEK-CNT nanocomposite filaments, not printed parts. Dul et al. [49] applied the Halpin–Tsai (HT) model to predict the properties of CNT-ABS nanocomposite filaments.

There is an utmost necessity to have efficient and accurate models to eliminate the experimental characterisation of such nanocomposites. Sheikh et al. [156], in a review work, discussed many computational methods and models of composites and nanocomposites. The models can be used in a hierarchical way to create a multiscale computational framework. This will extract the necessary information from a smaller scale and transfer it to a higher scale to take the effect of micro- and nanoscale phenomena, such as agglomeration, dispersion, and aspect ratios, of nanofillers [157,158]. Eshelby–Mori–Tanaka (EMT) [159,160], a micromechanical computation model, has been used by researchers to

predict the nanofillers' effect in final polymer composites. The method does not capture the atomistic interactions of nanofillers and matrix aspect ratios. Another model, Halpin–Tsai (HT), is a simpler version of the EMT model, which takes account of the aspect ratio of the nanofillers but with no dispersion or agglomeration.

Sheikh et al. modelled and used a two-scale volume average homogenisation (VAM) and asymptotic homogenisation (AH) method to investigate neat polymers in the fused deposition modelling parts as laminated composites [22,23,93,161]. In another study, Aslan et al. [162,163] investigated neat polymers using a homogenisation technique. Since these methods have been used for neat polymers in the FDM technique, a proper combination of atomistic- or micro-scale methods, such as EMT and HT in a hierarchical framework, could be a possible computational model to investigate FDM nanocomposites parts in the near future for novel application areas such as environmental air quality sensing [164–166].

5. Concluding Remarks

The method of choice among mechanical melt mixing, solutions, or local enrichment must be selected properly because melt mixing is fast, simple, and easy to operate in comparison to the solution-based method. However the former faces challenges in the proper homogeneously dispersion of nanofillers in the polymer matrix. The latter involves sonication and dispersion in solvents and, therefore, produces less agglomeration in the final nanocomposites. The chemical solution method involving chemicals is not pleasant to choose, and therefore, as reviewed in this work, tabulated in Table 1, most of the researchers are choosing the melt-mixing method, but all these works are focused on research-based study. For industrial acceptance, which method should be opted for?

Local enrichment is another technique presented by a few researchers, as discussed in this study. The advantage of this method is demonstrated by the improved properties of the FDM-printed part in comparison to the conventionally prepared (melt-mixing chemical solution) method. The point of interest is that this method does not involve the bulk dispersion of nanofillers but a deposited layer over the polymer. Therefore, it can be said that the filament is a sandwiched structure rather than a proper bulk composite. Since the demonstrated properties are many-fold enhanced, only a few studies have been presented in the literature, and therefore, this must be properly and heavily investigated for wide acceptance, as with the other two methods.

In the chemical solution method, one of the biggest challenges to face is to wait for the preparation of sheets of nanocomposites before they can be processed into filaments. In the literature, all the studies have used the spreading of the nanocomposite solution mix into sheets of the required thickness. This step needs more time, about 24 h or more, to let the solvent evaporate. Furthermore, extra heating is necessary to remove the solvent, or else it will create porosity in the filament, distorting the diameter consistency. Therefore, new or substitute techniques must arrive to expedite this step in improving the filament quality.

Filament processing involves parameters such as the pellet size of feedstock, the moisture content in pellets, the temperature profile, and the cooling medium. These parameters are not much discussed in the literature, which is of utmost importance because they control the printability of the filament. If the particle size is not consistent, it will affect the feed-in rate, creating a difference in the inflow of mass and outflow of mass into the extruder and from the extruder, respectively. The pulling speed of the filament must be controlled because if pulled too fast, the diameter will be decreased, and pulling too fast will increase the filament diameter. A proper database or a standard must be created that signifies the required processing temperature corresponding to every nanofiller and matrix combination. The extruding parameters also control the orientation of the nanofillers in the polymer matrix, which affects the percolation network and the final performance of the FDM-printed part.

The discussed nanofillers, CNTs, graphene, and cellulose overall improve the properties, thermal, mechanical, or electrical. There are some studies that were reviewed that demonstrated the detrimental effect on the performance of the final printed nanocomposites.

The attributed reason is the biggest challenge regarding the agglomeration and percolation at low concentrations of nanofillers in the polymer matrix. This study exhaustively reviewed and presented studies that investigated these challenges and tried to improve the final properties, but it was still a challenge. The proper dispersion and agglomeration are affected by the processing method used to make nanocomposite filaments in the extruder, along with the extrusion parameters. Therefore, it is of utmost importance to choose and select the proper parameters while processing the nanocomposites.

A comparative study is needed for the three stages of the FDM technique: (i) The fabrication of nanocomposites, (ii) the fabrication of the filaments, and (iii) the printing of the part. In all these stages, the nanocomposite undergoes melting and solidifying. Therefore, the effect of the temperature in all these steps needs to be studied completely and properly. The filler's orientation, agglomeration, and dispersion could be affected by multiple melting and solidification.

Author Contributions: T.S.: conceptualization, writing—original draft, review, and editing. K.B.: conceptualization, supervision, and writing—review and editing. All authors have read and agreed to the published version of the manuscript.

Funding: The funding received for this research is from The Natural Science and Engineering Research Council of Canada (NSERC under grant RGPIN-217525).

Acknowledgments: Support from the Advanced Research Laboratory Multifunctional Lightweight Structures (ARL-MLS), University of Toronto, is greatly acknowledged.

Conflicts of Interest: The authors declare that they have no known competing financial interests or personal relationships that could have appeared to influence the work reported in this paper.

References

1. Sztorch, B.; Brząkalski, D.; Pakuła, D.; Frydrych, M.; Špitalský, Z.; Przekop, R.E. Natural and Synthetic Polymer Fillers for Applications in 3D Printing—FDM Technology Area. *Solids* **2022**, *3*, 508–548. [CrossRef]
2. Hull, C.W. Apparatus for Production of Three-Dimensional Objects by Stereolithography. U.S. Patent US4575330A, 11 March 1986.
3. Ngo, T.D.; Kashani, A.; Imbalzano, G.; Nguyen, K.T.Q.; Hui, D. Additive manufacturing (3D printing): A review of materials, methods, applications and challenges. *Compos. Part B Eng.* **2018**, *143*, 172–196. [CrossRef]
4. Iqbal, A.; Saeed, A.; Ul-Hamid, A. A review featuring the fundamentals and advancements of polymer/CNT nanocomposite application in aerospace industry. *Polym. Bull.* **2020**, *78*, 539–557. [CrossRef]
5. Han, D.; Lee, H. Recent advances in multi-material additive manufacturing: Methods and applications. *Curr. Opin. Chem. Eng.* **2020**, *28*, 158–166. [CrossRef]
6. Liravi, F.; Toyserkani, E. Additive manufacturing of silicone structures: A review and prospective. *Addit. Manuf.* **2018**, *24*, 232–242. [CrossRef]
7. Dizon, J.R.C.; Espera, A.H., Jr.; Chen, Q.; Advincula, R.C. Mechanical characterization of 3D-printed polymers. *Addit. Manuf.* **2018**, *20*, 44–67. [CrossRef]
8. Vaidya, A.A.; Collet, C.; Gaugler, M.; Lloyd-Jones, G. Integrating softwood biorefinery lignin into polyhydroxybutyrate composites and application in 3D printing. *Mater. Today Commun.* **2019**, *19*, 286–296. [CrossRef]
9. Mazzanti, V.; Malagutti, L.; Mollica, F. FDM 3D Printing of Polymers Containing Natural Fillers: A Review of their Mechanical Properties. *Polymers* **2019**, *11*, 1094. [CrossRef]
10. Grand View Research. *3D Printing Market Size, Share & Trends Analysis Report by Component (Hardware, Software, Services), by Printer Type, by Technology, by Software, by Application, by Vertical, by Region, and Segment Forecasts Dublin, Ireland*; Grand View Research: San Francisco, CA, USA, 2022.
11. Chohan, J.S.; Kumar, R.; Singh, S.; Sharma, S.; Ilyas, R.A. A comprehensive review on applications of 3D printing in natural fibers polymer composites for biomedical applications. *Funct. Compos. Struct.* **2022**, *4*, 034001. [CrossRef]
12. Montez, M.; Willis, K.; Rendler, H.; Marshall, C.; Rubio, E.; Rajak, D.K.; Rahman, M.H.; Menezes, P.L. Fused deposition model-ing (FDM): Processes, material properties, and applications. In *Tribology of Additively Manufactured Materials*; Elsevier: Amsterdam, The Netherlands, 2022; pp. 137–163. [CrossRef]
13. Chandrasekar, R.; Gkantou, M.; Nikitas, G.; Hashim, K.; Pradeep, H.R.; Ahuja, A. Integration of 3D Concrete Printing in the Construction Industry: A Short Review. In *Current Trends in Geotechnical Engineering and Construction*; Springer: Singapore, 2023; pp. 445–452. [CrossRef]
14. Salifu, S.; Desai, D.; Ogunbiyi, O.; Mwale, K. Recent development in the additive manufacturing of polymer-based composites for automotive structures—A review. *Int. J. Adv. Manuf. Technol.* **2022**, *119*, 6877–6891. [CrossRef]

15. Vyavahare, S.; Teraiya, S.; Panghal, D.; Kumar, S. Fused deposition modelling: A review. *Rapid Prototyp. J.* **2020**, *26*, 176–201. [CrossRef]
16. Hassanifard, S.; Behdinan, K. Effects of voids and raster orientations on fatigue life of notched additively manufactured PLA components. *Int. J. Adv. Manuf. Technol.* **2022**, *120*, 6241–6250. [CrossRef]
17. Divakaran, N.; Kumar, P.V.A.; Mohapatra, A.; Alex, Y.; Mohanty, S. Significant Role of Carbon Nanomaterials in Material Extrusion-Based 3D-Printed Triboelectric Nanogenerators. *Energy Technol.* **2023**, *11*, 2201275. [CrossRef]
18. Chapa, A.; Cuan-Urquizo, E.; Urbina-Coronado, P.; Roman-Flores, A. Experimental characterization of the mechanical properties of 3D printed TPU auxetic cellular materials under cyclic compressive loadings. *Rapid Prototyp. J.* **2023**, *29*, 1800–1813. [CrossRef]
19. Penumakala, P.K.; Santo, J.; Thomas, A. A critical review on the fused deposition modeling of thermoplastic polymer composites. *Compos. Part B Eng.* **2020**, *201*, 108336. [CrossRef]
20. Cuan-Urquizo, E.; Barocio, E.; Tejada-Ortigoza, V.; Pipes, R.B.; Rodriguez, C.A.; Roman-Flores, A. Characterization of the mechanical properties of FFF structures and materials: A review on the experimental, computational and theoretical approaches. *Materials* **2019**, *12*, 895. [CrossRef]
21. Sheoran, A.J.; Kumar, H. Fused Deposition modeling process parameters optimization and effect on mechanical properties and part quality: Review and reflection on present research. *Mater. Today Proc.* **2019**, *21*, 1659–1672. [CrossRef]
22. Sheikh, T.; Behdinan, K. Geometric void-multiscale model for evaluating the effect of bead width and layer height on voids in FDM parts. *Rapid Prototyp. J.* **2023**, *29*, 1565–1579. [CrossRef]
23. Sheikh, T.; Behdinan, K. The effect of process parameters on the mechanical properties of additively manufactured parts using a hierarchical multiscale model. *Rapid Prototyp. J.* **2022**, *29*, 1029–1043. [CrossRef]
24. Angelopoulos, P.M.; Samouhos, M.; Taxiarchou, M. Functional fillers in composite filaments for fused filament fabrication; a review. *Mater. Today Proc.* **2021**, *37*, 4031–4043. [CrossRef]
25. Lee, C.H.; Padzil, F.N.B.M.; Lee, S.H.; Ainun, Z.M.A.; Abdullah, L.C. Potential for Natural Fiber Reinforcement in PLA Polymer Filaments for Fused Deposition Modeling (FDM) Additive Manufacturing: A Review. *Polymers* **2021**, *13*, 1407. [CrossRef]
26. Gama, N.; Magina, S.; Barros-Timmons, A.; Ferreira, A. Enhanced compatibility between coconut fibers/PP via chemical mod-ification for 3D printing. *Prog. Addit. Manuf.* **2022**, *7*, 213–223. [CrossRef]
27. Ahmad, M.N.; Ishak, M.R.; Taha, M.M.; Mustapha, F.; Leman, Z. Rheological Properties of Natural Fiber Reinforced Thermoplastic Composite for Fused Deposition Modeling (FDM): A Short Review. *J. Adv. Res. Fluid Mech. Therm. Sci.* **2022**, *98*, 157–164. [CrossRef]
28. Almuallim, B.; Harun, W.S.W.; Al Rikabi, I.J.; Mohammed, H.A. Thermally conductive polymer nanocomposites for fila-ment-based additive manufacturing. *J. Mater. Sci.* **2022**, *57*, 3993–4019. [CrossRef]
29. Sandanamsamy, L.; Harun, W.S.W.; Ishak, I.; Romlay, F.R.M.; Kadirgama, K.; Ramasamy, D.; Idris, S.R.A.; Tsumori, F. A comprehensive review on fused deposition modelling of polylactic acid. *Prog. Addit. Manuf.* **2022**, *8*, 775–799. [CrossRef]
30. Parnian, P. A Short Review on: Recent Advances in the Use of Carbon Nanotubes in Additive Manufacturing of Polymer Matrix Composites. *Macromol. Symp.* **2022**, *405*, 2100339. [CrossRef]
31. Roudný, P.; Syrový, T. Thermal conductive composites for FDM 3D printing: A review, opportunities and obstacles, future directions. *J. Manuf. Process.* **2022**, *83*, 667–677. [CrossRef]
32. Park, S.; Fu, K. Polymer-based filament feedstock for additive manufacturing. *Compos. Sci. Technol.* **2021**, *213*, 108876. [CrossRef]
33. 3D Printer Filament 1.75 mm vs. 3 mm—All You Need To Know—3D Printerly. 2022. Available online: https://3dprinterly.com/3d-printer-filament-1-75mm-vs-3mm-all-you-need-to-know/ (accessed on 9 November 2022).
34. Gibson, I.; Rosen, D.W.; Stucker, B. Extrusion-Based Systems. In *Additive Manufacturing Technologies*; Springer: Boston, MA, USA, 2010; pp. 160–186. [CrossRef]
35. Elbadawi, M. Polymeric Additive Manufacturing: The Necessity and Utility of Rheology. In *Polymer Rheology*; IntechOpen: London, UK, 2018. [CrossRef]
36. Rahim, T.N.A.T.; Abdullah, A.M.; Akil, H.M. Recent Developments in Fused Deposition Modeling-Based 3D Printing of Polymers and Their Composites. *Polym. Rev.* **2019**, *59*, 589–624. [CrossRef]
37. Berretta, S.; Davies, R.; Shyng, Y.; Wang, Y.; Ghita, O. Fused Deposition Modelling of high temperature polymers: Exploring CNT PEEK composites. *Polym. Test.* **2017**, *63*, 251–262. [CrossRef]
38. Peng, F.; Jiang, H.; Woods, A.; Joo, P.; Amis, E.J.; Zacharia, N.S.; Vogt, B.D. 3D Printing with Core–Shell Filaments Containing High or Low Density Polyethylene Shells. *ACS Appl. Polym. Mater.* **2019**, *1*, 275–285. [CrossRef]
39. Wang, T.-M.; Xi, J.-T.; Jin, Y. A model research for prototype warp deformation in the FDM process. *Int. J. Adv. Manuf. Technol.* **2006**, *33*, 1087–1096. [CrossRef]
40. Hart, K.R.; Dunn, R.M.; Wetzel, E.D. Tough, Additively Manufactured Structures Fabricated with Dual-Thermoplastic Filaments. *Adv. Eng. Mater.* **2020**, *22*, 1901184. [CrossRef]
41. Rajan, K.; Samykano, M.; Kadirgama, K.; Harun, W.S.W.; Rahman, M. Fused deposition modeling: Process, materials, parameters, properties, and applications. *Int. J. Adv. Manuf. Technol.* **2022**, *120*, 1531–1570. [CrossRef]
42. Peng, Z.; Lv, Q.; Jing, J.; Pei, H.; Chen, Y.; Ivanov, E. FDM-3D printing LLDPE/BN@GNPs composites with double network structures for high-efficiency thermal conductivity and electromagnetic interference shielding. *Compos. Part B Eng.* **2023**, *251*, 110491. [CrossRef]

43. Wang, Q.; Ji, C.; Sun, L.; Sun, J.; Liu, J. Cellulose Nanofibrils Filled Poly(Lactic Acid) Biocomposite Filament for FDM 3D Printing. *Molecules* **2020**, *25*, 2319. [CrossRef]
44. Zhuang, Y.; Song, W.; Ning, G.; Sun, X.; Sun, Z.; Xu, G.; Zhang, B.; Chen, Y.; Tao, S. 3D–printing of materials with anisotropic heat distribution using conductive polylactic acid composites. *Mater. Des.* **2017**, *126*, 135–140. [CrossRef]
45. Zare, Y. Study of nanoparticles aggregation/agglomeration in polymer particulate nanocomposites by mechanical properties. *Compos. Part A Appl. Sci. Manuf.* **2016**, *84*, 158–164. [CrossRef]
46. Podsiadły, B.; Matuszewski, P.; Skalski, A.; Słoma, M. Carbon Nanotube-Based Composite Filaments for 3D Printing of Structural and Conductive Elements. *Appl. Sci.* **2021**, *11*, 1272. [CrossRef]
47. Shi, S.; Peng, Z.; Jing, J.; Yang, L.; Chen, Y. 3D Printing of Delicately Controllable Cellular Nanocomposites Based on Polylac-tic Acid Incorporating Graphene/Carbon Nanotube Hybrids for Efficient Electromagnetic Interference Shielding. *ACS Sustain. Chem. Eng.* **2020**, *8*, 7962–7972. [CrossRef]
48. Shi, S.; Chen, Y.; Jing, J.; Yang, L. Preparation and 3D-printing of highly conductive polylactic acid/carbon nanotube nanocomposites via local enrichment strategy. *RSC Adv.* **2019**, *9*, 29980–29986. [CrossRef]
49. Dul, S.; Gutierrez, B.J.A.; Pegoretti, A.; Alvarez-Quintana, J.; Fambri, L. 3D printing of ABS Nanocomposites. Comparison of processing and effects of multi-wall and single-wall carbon nanotubes on thermal, mechanical and electrical properties. *J. Mater. Sci. Technol.* **2022**, *121*, 52–66. [CrossRef]
50. Dul, S.; Pegoretti, A.; Fambri, L. Effects of the Nanofillers on Physical Properties of Acrylonitrile-Butadiene-Styrene Nanocomposites: Comparison of Graphene Nanoplatelets and Multiwall Carbon Nanotubes. *Nanomaterials* **2018**, *8*, 674. [CrossRef]
51. Jing, J.; Chen, Y.; Shi, S.; Yang, L.; Lambin, P. Facile and scalable fabrication of highly thermal conductive polyethylene/graphene nanocomposites by combining solid-state shear milling and FDM 3D-printing aligning methods. *Chem. Eng. J.* **2020**, *402*, 126218. [CrossRef]
52. Huang, X.; Panahi-Sarmad, M.; Dong, K.; Cui, Z.; Zhang, K.; Gonzalez, O.G.; Xiao, X. 4D printed TPU/PLA/CNT wave structural composite with intelligent thermal-induced shape memory effect and synergistically enhanced mechanical properties. *Compos. Part A Appl. Sci. Manuf.* **2022**, *158*, 106946. [CrossRef]
53. Tan, D.K.; Maniruzzaman, M.; Nokhodchi, A. Advanced Pharmaceutical Applications of Hot-Melt Extrusion Coupled with Fused Deposition Modelling (FDM) 3D Printing for Personalised Drug Delivery. *Pharmaceutics* **2018**, *10*, 203. [CrossRef]
54. Spinelli, G.; Kotsilkova, R.; Ivanov, E.; Petrova-Doycheva, I.; Menseidov, D.; Georgiev, V.; Di Maio, R.; Silvestre, C. Effects of Filament Extrusion, 3D Printing and Hot-Pressing on Electrical and Tensile Properties of Poly(Lactic) Acid Composites Filled with Carbon Nanotubes and Graphene. *Nanomaterials* **2019**, *10*, 35. [CrossRef]
55. Goh, G.L.; Agarwala, S.; Yeong, W.Y. Directed and On-Demand Alignment of Carbon Nanotube: A Review toward 3D Printing of Electronics. *Adv. Mater. Interfaces* **2019**, *6*, 1801318. [CrossRef]
56. Mercator, Z. Single Screw Extruder. 2022. Available online: https://www.masterlabsrl.it/wp-content/uploads/2021/04/Zamak-catalogo.pdf (accessed on 11 July 2022).
57. Patil, H.; Tiwari, R.V.; Repka, M.A. Hot-Melt Extrusion: From Theory to Application in Pharmaceutical Formulation. *AAPS PharmSciTech* **2016**, *17*, 20–42. [CrossRef]
58. Crowley, M.M.; Zhang, F.; Repka, M.A.; Thumma, S.; Upadhye, S.B.; Battu, S.K.; McGinity, J.W.; Martin, C. Pharmaceutical Applications of Hot-Melt Extrusion: Part I. *Drug Dev. Ind. Pharm.* **2008**, *33*, 909–926. [CrossRef]
59. Shrivastava, A. Plastics Processing. In *Applied Plastics Engineering Handbook: Processing and Materials*; Elsevier: Amsterdam, The Netherlands, 2018; pp. 143–177. [CrossRef]
60. Meet the Composer and Precision—Desktop Filament Makers. 3devo, (n.d.). Available online: https://www.3devo.com/filament-makers (accessed on 7 November 2022).
61. Chen, Q.; Mangadlao, J.D.; Wallat, J.; De Leon, A.; Pokorski, J.K.; Advincula, R.C. 3D printing biocompatible polyurethane/poly(lactic acid)/graphene oxide nanocomposites: Anisotropic properties. *ACS Appl. Mater. Interfaces* **2017**, *9*, 4015–4023. [CrossRef]
62. Caminero, M.Á.; Chacón, J.M.; García-Plaza, E.; Núñez, P.J.; Reverte, J.M.; Becar, J.P. Additive Manufacturing of PLA-Based Composites Using Fused Filament Fabrication: Effect of Graphene Nanoplatelet Reinforcement on Mechanical Properties, Dimensional Accuracy and Texture. *Polymers* **2019**, *11*, 799. [CrossRef]
63. Ryan, K.R.; Down, M.P.; Hurst, N.J.; Keefe, E.M.; Banks, C.E. Additive manufacturing (3D printing) of electrically conductive polymers and polymer nanocomposites and their applications. *eScience* **2022**, *2*, 365–381. [CrossRef]
64. Gnanasekaran, K.; Heijmans, T.; van Bennekom, S.; Woldhuis, H.; Wijnia, S.; de With, G.; Friedrich, H. 3D printing of CNT- and graphene-based conductive polymer nanocomposites by fused deposition modeling. *Appl. Mater. Today* **2017**, *9*, 21–28. [CrossRef]
65. Lyu, Z.; Lim, G.J.; Koh, J.J.; Li, Y.; Ma, Y.; Ding, J.; Wang, J.; Hu, Z.; Wang, J.; Chen, W.; et al. Design and Manufacture of 3D-Printed Batteries. *Joule* **2021**, *5*, 89–114. [CrossRef]
66. Ni, Y.; Ji, R.; Long, K.; Bu, T.; Chen, K.; Zhuang, S. A review of 3D-printed sensors. *Appl. Spectrosc. Rev.* **2017**, *52*, 623–652. [CrossRef]
67. Oran, S.; Toprakci, H.A.K.; Toprakci, O.; Tasdelen, M.A. Multi-walled Carbon Nanotube/Acrylonitrile Butadiene Sty-rene Nanocomposite Filaments for Fused Deposition Modelling Type 3D Printing. *Chem. Afr.* **2022**, *5*, 2259–2269. [CrossRef]
68. Dul, S.; Fambri, L.; Pegoretti, A. Filaments Production and Fused Deposition Modelling of ABS/Carbon Nanotubes Composites. *Nanomaterials* **2018**, *8*, 49. [CrossRef] [PubMed]

69. Jindal, P.; Jyoti, J.; Kumar, N. Mechanical characterisation of ABS/MWCNT composites under static and dynamic loading conditions. *J. Mech. Eng. Sci.* **2016**, *10*, 2288–2299. [CrossRef]
70. Pour, R.H.; Hassan, A.; Soheilmoghaddam, M.; Bidsorkhi, H.C. Mechanical, thermal, and morphological properties of graphene reinforced polycarbonate/acrylonitrile butadiene styrene nanocomposites. *Polym. Compos.* **2016**, *37*, 1633–1640. [CrossRef]
71. Le, T.-H.; Le, V.-S.; Dang, Q.-K.; Nguyen, M.-T.; Le, T.-K.; Bui, N.-T. Microstructure Evaluation and Thermal–Mechanical Properties of ABS Matrix Composite Filament Reinforced with Multi-Walled Carbon Nanotubes by a Single Screw Extruder for FDM 3D Printing. *Appl. Sci.* **2021**, *11*, 8798. [CrossRef]
72. Wang, B.; Chen, Y.; Qu, T.; Li, F. Structure and Properties of Multi-walled Carbon Nanotube/Acrylonitrile Butadiene Styrene Nanocomposite Specimens Prepared by Fused Deposition Modeling. *J. Macromol. Sci. Part B* **2020**, *60*, 77–87. [CrossRef]
73. Meng, S.; He, H.; Jia, Y.; Yu, P.; Huang, B.; Chen, J. Effect of nanoparticles on the mechanical properties of acrylonitrile–butadiene–styrene specimens fabricated by fused deposition modeling. *J. Appl. Polym. Sci.* **2017**, *134*, 44470. [CrossRef]
74. Nadernezhad, A.; Unal, S.; Khani, N.; Koc, B. Material extrusion-based additive manufacturing of structurally controlled poly(lactic acid)/carbon nanotube nanocomposites. *Int. J. Adv. Manuf. Technol.* **2019**, *102*, 2119–2132. [CrossRef]
75. Xiang, Z.; Chen, T.; Li, Z.; Bian, X. Negative Temperature Coefficient of Resistivity in Lightweight Conductive Carbon Nanotube/Polymer Composites. *Macromol. Mater. Eng.* **2009**, *294*, 91–95. [CrossRef]
76. Radzuan, N.A.M.; Sulong, A.B.; Hui, D.; Verma, A. Electrical Conductivity Performance of Predicted Modified Fibre Contact Model for Multi-Filler Polymer Composite. *Polymers* **2019**, *11*, 1425. [CrossRef]
77. Tang, H.; Chen, X.; Luo, Y. Studies on the PTC/NTC effect of carbon black filled low density polyethylene composites. *Eur. Polym. J.* **1997**, *33*, 1383–1386. [CrossRef]
78. Sezer, H.K.; Eren, O. FDM 3D printing of MWCNT re-inforced ABS nano-composite parts with enhanced mechanical and electrical properties. *J. Manuf. Process.* **2019**, *37*, 339–347. [CrossRef]
79. Pan, S.; Shen, H.; Zhang, L. Effect of carbon nanotube on thermal, tribological and mechanical properties of 3D printing polyphenylene sulfide. *Addit. Manuf.* **2021**, *47*, 102247. [CrossRef]
80. Wang, Y.; Yang, C.; Xin, Z.; Luo, Y.; Wang, B.; Feng, X.; Mao, Z.; Sui, X. Poly(lactic acid)/carbon nanotube composites with enhanced electrical conductivity via a two-step dispersion strategy. *Compos. Commun.* **2022**, *30*, 101087. [CrossRef]
81. Deepak, J.; Adarsha, H.; Keshavamurthy, R.; Ramkumar, N.P. Analysis of Thermal Behaviour of Carbon Nano-tubes-Reinforced HDPE Composites Developed Using FDM Process. *J. Inst. Eng. (India) Ser. D* **2023**, 1–13. [CrossRef]
82. Han, B.; Wang, Y.; Zheng, Y.; Tao, Y.; Liu, X. Influence of multi-walled carbon nanotube content on electromagnetic wave absorption and mechanical properties of carbon nanotube/polyamide 12 composite. *Polym. Compos.* **2022**, *43*, 7739–7750. [CrossRef]
83. Sheikh, T.; Sampath, S.; Bhattacharya, B. Bimorph sensor based in-line inspection method for corrosion defect detection in natural gas pipelines. *Sensors Actuators A Phys.* **2022**, *347*, 113940. [CrossRef]
84. Sheikh, T.; Sampath, S.; Bhattacharya, B. Analytical study on the effects of geometrical parameters on the bimorph sensor performance to detect surface defects in gas pipelines. In *ACAM10: 10th Australasian Congress on Applied Mechanics*; Engineering Australia: Canberra, Australia, 2021; pp. 322–332.
85. Li, Y.; Zheng, L.; Song, L.; Han, Y.; Yang, Y.; Tan, C. Toward Balanced Piezoelectric and Mechanical Performance: 3D Printed Polyvinylidene Fluoride/Carbon Nanotube Energy Harvester with Hierarchical Structure. *Ind. Eng. Chem. Res.* **2022**, *61*, 13063–13071. [CrossRef]
86. Verma, P.; Ubaid, J.; Varadarajan, K.M.; Wardle, B.L.; Kumar, S. Synthesis and Characterization of Carbon Nanotube-Doped Thermoplastic Nanocomposites for the Additive Manufacturing of Self-Sensing Piezoresistive Materials. *ACS Appl. Mater. Interfaces* **2022**, *14*, 8361–8372. [CrossRef]
87. Chen, Q.; Zhang, Y.-Y.; Huang, P.; Li, Y.-Q.; Fu, S.-Y. Improved bond strength, reduced porosity and enhanced mechanical properties of 3D-printed polyetherimide composites by carbon nanotubes. *Compos. Commun.* **2022**, *30*, 101083. [CrossRef]
88. Petousis, M.; Ninikas, K.; Vidakis, N.; Mountakis, N.; Kechagias, J.D. Multifunctional PLA/CNTs nanocomposites hybrid 3D printing integrating material extrusion and CO_2 laser cutting. *J. Manuf. Process.* **2023**, *86*, 237–252. [CrossRef]
89. Kotsilkova, R.; Tabakova, S. Exploring Effects of Graphene and Carbon Nanotubes on Rheology and Flow Instability for Designing Printable Polymer Nanocomposites. *Nanomaterials* **2023**, *13*, 835. [CrossRef]
90. Yang, L.; Liu, X.; Xiao, Y.; Liu, B.; Xue, Z.; Wang, Y. Additive manufacturing of carbon nanotube/polylactic acid films with efficient electromagnetic interference shielding and electrical heating performance via fused deposition modeling. *Synth. Met.* **2023**, *293*, 117258. [CrossRef]
91. Yang, L.; Li, S.; Zhou, X.; Liu, J.; Li, Y.; Yang, M.; Yuan, Q.; Zhang, W. Effects of carbon nanotube on the thermal, mechanical, and electrical properties of PLA/CNT printed parts in the FDM process. *Synth. Met.* **2019**, *253*, 122–130. [CrossRef]
92. De Bortoli, L.; de Farias, R.; Mezalira, D.; Schabbach, L.; Fredel, M. Functionalized carbon nanotubes for 3D-printed PLA-nanocomposites: Effects on thermal and mechanical properties. *Mater. Today Commun.* **2022**, *31*, 103402. [CrossRef]
93. Sheikh, T.; Behdinan, K. Multiscale Analysis of Laminates Printed by 3D Printing Fused Deposition Modeling Method. In *Advanced Composite Materials and Structures*; CRC Press: Boca Raton, FL, USA, 2022; pp. 233–243. [CrossRef]
94. Wallin, T.J.; Pikul, J.; Shepherd, R.F. 3D printing of soft robotic systems. *Nat. Rev. Mater.* **2018**, *3*, 84–100. [CrossRef]

95. Tzounis, L.; Petousis, M.; Grammatikos, S.; Vidakis, N. 3D Printed Thermoelectric Polyurethane/Multiwalled Carbon Nanotube Nanocomposites: A Novel Approach towards the Fabrication of Flexible and Stretchable Organic Thermoelectrics. *Materials* **2020**, *13*, 2879. [CrossRef]
96. Li, B.; Liang, W.; Zhang, L.; Ren, F.; Xuan, F. TPU/CNTs flexible strain sensor with auxetic structure via a novel hybrid manufacturing process of fused deposition modeling 3D printing and ultrasonic cavitation-enabled treatment. *Sens. Actuators A Phys.* **2022**, *340*, 113526. [CrossRef]
97. Pan, H.; Wang, Z.; Wei, Z.; Zhang, J.; Xu, M.; Zong, C.; Cao, L.; Wang, Q. Sandwiched-resistive sensors based on the 3D printing of TPU/CNTs–ILs. *J. Mater. Sci.* **2022**, *57*, 9187–9201. [CrossRef]
98. Candal, M.V.; Calafel, I.; Fernández, M.; Aranburu, N.; Aguirresarobe, R.H.; Gerrica-Echevarria, G.; Santamaría, A.; Müller, A.J. Study of the interlayer adhesion and warping during material extrusion-based additive manufacturing of a carbon nanotube/biobased thermoplastic polyurethane nanocomposite. *Polymer* **2021**, *224*, 123734. [CrossRef]
99. Farajian, J.; Alipanahi, A.; Mahboubkhah, M. Analyses of mechanical properties and morphological behavior of additively manufactured ABS polymer, ABS/PBT blend, and ABS/PBT/CNT nanocomposite parts. *J. Thermoplast. Compos. Mater.* **2022**, *36*, 2390–2411. [CrossRef]
100. Kiranakumar, H.V.; Thejas, R.; Naveen, C.S.; Khan, M.I.; Prasanna, G.D.; Reddy, S.; Oreijah, M.; Guedri, K.; Bafakeeh, O.T.; Jameel, M. A review on electrical and gas-sensing properties of reduced graphene oxide-metal oxide nanocomposites. *Biomass Convers. Biorefinery* **2022**, 1–11. [CrossRef]
101. Bilisik, K.; Akter, M. Graphene nanocomposites: A review on processes, properties, and applications. *J. Ind. Text.* **2022**, *51*, 3718S–3766S. [CrossRef]
102. Kausar, A.; Ahmad, I.; Zhao, T.; Aldaghri, O.; Eisa, M.H. Polymer/Graphene Nanocomposites via 3D and 4D Printing—Design and Technical Potential. *Processes* **2023**, *11*, 868. [CrossRef]
103. Mohanavel, V.; Kannan, S.; Mohan, R.; Arul, K.; Seikh, A.H.; Iqbal, A. Impact of CNT addition on Surface Roughness and Di-mensional Characteristics of Polymer Nano-Composite Fabricated by FDM method. *Int. J. Adv. Manuf. Technol.* **2023**. [CrossRef]
104. Muñoz, J.; La Cruz, J.O.-D.; Forte, G.; Pumera, M. Graphene-based 3D-Printed nanocomposite bioelectronics for monitoring breast cancer cell adhesion. *Biosens. Bioelectron.* **2023**, *226*, 115113. [CrossRef]
105. Camargo, J.C.; Machado, A.R.; Almeida, E.C.; de Almeida, V.H.M. Mechanical and electrical behavior of ABS polymer rein-forced with graphene manufactured by the FDM process. *Int. J. Adv. Manuf. Technol.* **2022**, *119*, 1019–1033. [CrossRef]
106. Tambrallimath, V.; Keshavamurthy, R.; Saravanabavan, D.; Badari, A.; Jeevan, M. Numerical and experimental analysis of thermal conductivity of PC-ABS nanocomposite reinforced with graphene developed by fused deposition modeling. *Mater. Today Proc.* **2021**, *46*, 8964–8967. [CrossRef]
107. Garzón, C.; Palza, H. Electrical behavior of polypropylene composites melt mixed with carbon-based particles: Effect of the kind of particle and annealing process. *Compos. Sci. Technol.* **2014**, *99*, 117–123. [CrossRef]
108. Hu, Z.; Li, N.; Li, J.; Zhang, C.; Song, Y.; Li, X.; Wu, G.; Xie, F.; Huang, Y. Facile preparation of poly(p-phenylene benzobisoxazole)/graphene composite films via one-pot in situ polymerization. *Polymer* **2015**, *71*, 8–14. [CrossRef]
109. Tambrallimath, V.; Keshavamurthy, R.; Bavan, S.D.; Patil, A.Y.; Khan, T.M.Y.; Badruddin, I.A.; Kamangar, S. Mechanical Properties of PC-ABS-Based Graphene-Reinforced Polymer Nanocomposites Fabricated by FDM Process. *Polymers* **2021**, *13*, 2951. [CrossRef]
110. Parviz, D.; Metzler, S.D.; Das, S.; Irin, F.; Green, M.J. Tailored Crumpling and Unfolding of Spray-Dried Pristine Graphene and Graphene Oxide Sheets. *Small* **2015**, *11*, 2661–2668. [CrossRef] [PubMed]
111. Santo, J.; Moola, A.R.; Penumakala, P.K. Interface stress transfer in an extruded ABS-rGO composite filament. *Adv. Compos. Mater.* **2022**, *32*, 211–224. [CrossRef]
112. Bonab, V.S.; Maxian, O.; Manas-Zloczower, I. Carbon nanofiller networks—A comparative study of networks formed by branched versus linear carbon nanotubes in thermoplastic polyurethane. *Polymer* **2019**, *175*, 227–234. [CrossRef]
113. Lanticse, L.J.; Tanabe, Y.; Matsui, K.; Kaburagi, Y.; Suda, K.; Hoteida, M.; Endo, M.; Yasuda, E. Shear-induced preferential alignment of carbon nanotubes resulted in anisotropic electrical conductivity of polymer composites. *Carbon* **2006**, *44*, 3078–3086. [CrossRef]
114. Starý, Z.; Krückel, J. Conductive polymer composites with carbonic fillers: Shear induced electrical behaviour. *Polymer* **2018**, *139*, 52–59. [CrossRef]
115. Shmueli, Y.; Lin, Y.-C.; Zuo, X.; Guo, Y.; Lee, S.; Freychet, G.; Zhernenkov, M.; Kim, T.; Tannenbaum, R.; Marom, G.; et al. In-situ X-ray scattering study of isotactic polypropylene/graphene nanocomposites under shear during fused deposition modeling 3D printing. *Compos. Sci. Technol.* **2020**, *196*, 108227. [CrossRef]
116. Ivanov, E.; Kotsilkova, R.; Xia, H.; Chen, Y.; Donato, R.K.; Donato, K.; Godoy, A.P.; Di Maio, R.; Silvestre, C.; Cimmino, S.; et al. PLA/Graphene/MWCNT Composites with Improved Electrical and Thermal Properties Suitable for FDM 3D Printing Applications. *Appl. Sci.* **2019**, *9*, 1209. [CrossRef]
117. Ferrari, A.C.; Meyer, J.C.; Scardaci, V.; Casiraghi, C.; Lazzeri, M.; Mauri, F.; Piscanec, S.; Jiang, D.; Novoselov, K.S.; Roth, S.; et al. Raman spectrum of graphene and graphene layers. *Phys. Rev. Lett.* **2006**, *97*, 187401. [CrossRef] [PubMed]
118. Ferrari, A.C.; Basko, D.M. Raman spectroscopy as a versatile tool for studying the properties of graphene. *Nat. Nanotechnol.* **2013**, *8*, 235–246. [CrossRef] [PubMed]

119. Kurita, S.; Yoshimura, A.; Kawamoto, H.; Uchida, T.; Kojima, K.; Tachibana, M.; Molina-Morales, P.; Nakai, H. Raman spectra of carbon nanowalls grown by plasma-enhanced chemical vapor deposition. *J. Appl. Phys.* **2005**, *97*, 104320. [CrossRef]
120. Rao, A.M.; Chen, J.; Richter, E.; Schlecht, U.; Eklund, P.C.; Haddon, R.C.; Venkateswaran, U.D.; Kwon, Y.-K.; Tománek, D. Effect of van der Waals Interactions on the Raman Modes in Single Walled Carbon Nanotubes. *Phys. Rev. Lett.* **2001**, *86*, 3895–3898. [CrossRef]
121. Ivanov, E.; Kotsilkova, R.; Krusteva, E. Effect of processing on rheological properties and structure development of EPOXY/MWCNT nanocomposites. *J. Nanoparticle Res.* **2011**, *13*, 3393–3403. [CrossRef]
122. Wang, T.; Drzal, L.T. Cellulose-Nanofiber-Reinforced Poly(lactic acid) Composites Prepared by a Water-Based Approach. *ACS Appl. Mater. Interfaces* **2012**, *4*, 5079–5085. [CrossRef]
123. Liu, R.; Zhu, F.; Hu, J.; Li, J.; Han, J. Cellulose nanocrystals/water-based polyurethane nanocomposite films with excellent wear resistance and softness. *Micro Nano Lett.* **2021**, *16*, 268–273. [CrossRef]
124. Pathak, S.M.; Kumar, V.P.; Bonu, V.; Latha, S.; Mishnaevsky, L.; Lakshmi, R.; Bera, P.; Barshilia, H.C. Solid particle erosion studies of ceramic oxides reinforced water-based PU nanocomposite coatings for wind turbine blade protection. *Ceram. Int.* **2022**, *48*, 35788–35798. [CrossRef]
125. Carrola, M.; de Castro, E.M.; Tabei, A.; Asadi, A. Cellulose nanocrystal-assisted processing of nanocomposite filaments for fused filament fabrication. *Polymer* **2023**, *278*, 125980. [CrossRef]
126. Kusmono, N.D.A.; Herianto, M.W.W. Preparation and properties of cellulose nanocrystals-reinforced Poly (lactic acid) composite filaments for 3D printing applications. *Results Eng.* **2023**, *17*, 100842. [CrossRef]
127. Demir, M.; Seki, Y. Interfacial adhesion strength between FDM-printed PLA parts and surface-treated cellulosic-woven fabrics. *Rapid Prototyp. J.* **2023**, *29*, 1166–1174. [CrossRef]
128. Da Costa, F.A.T.; Parra, D.F.; Cardoso, E.C.L.; Güven, O. PLA, PBAT, Cellulose Nanocrystals (CNCs), and Their Blends: Biodegradation, Compatibilization, and Nanoparticle Interactions. *J. Polym. Environ.* **2023**, *31*, 4662–4690. [CrossRef]
129. Kumar, S.D.; Venkadeshwaran, K.; Aravindan, M. Fused deposition modelling of PLA reinforced with cellulose nano-crystals. *Mater. Today Proc.* **2020**, *33*, 868–875. [CrossRef]
130. Wang, Q.; Ji, C.; Sun, J.; Zhu, Q.; Liu, J. Structure and Properties of Polylactic Acid Biocomposite Films Reinforced with Cellulose Nanofibrils. *Molecules* **2020**, *25*, 3306. [CrossRef]
131. Talebi, H.; Ghasemi, F.A.; Ashori, A. The effect of nanocellulose on mechanical and physical properties of chitosan-based biocomposites. *J. Elastomers Plast.* **2022**, *54*, 22–41. [CrossRef]
132. Ling, Z.; Chen, J.; Wang, X.; Shao, L.; Wang, C.; Chen, S.; Guo, J.; Yong, Q. Nature-inspired construction of iridescent CNC/Nano-lignin films for UV resistance and ultra-fast humidity response. *Carbohydr. Polym.* **2022**, *296*, 119920. [CrossRef]
133. Aramian, A.; Razavi, N.; Sadeghian, Z.; Berto, F. A review of additive manufacturing of cermets. *Addit. Manuf.* **2020**, *33*, 101130. [CrossRef]
134. Wang, X.; Jiang, M.; Zhou, Z.W.; Gou, J.H.; Hui, D. 3D printing of polymer matrix composites: A review and prospective. *Compos. Part B Eng.* **2017**, *110*, 442–458. [CrossRef]
135. Agbakoba, V.C.; Hlangothi, P.; Andrew, J.; John, M.J. Mechanical and Shape Memory Properties of 3D-Printed Cellulose Nanocrystal (CNC)-Reinforced Polylactic Acid Bionanocomposites for Potential 4D Applications. *Sustainability* **2022**, *14*, 12759. [CrossRef]
136. Wu, X.; Liu, Y.; Wu, H.; Duan, Y.; Zhang, J. Melt-processed poly (L-lactic acid)/cellulose nanocrystals biocomposites for 3D printing: Improved melt processibility and inter-fuse adhesion. *Compos. Sci. Technol.* **2022**, *218*, 109135. [CrossRef]
137. Kusmono; Wiratma, O.E.R. Fabrication and Characterization of PLA/Nanocrystalline Cellulose Nanocomposite Filaments for 3D Printing Application. *IOP Conf. Series Mater. Sci. Eng.* **2021**, *1096*, 012055. [CrossRef]
138. Wu, X.; Liu, Y.-X.; Wu, H.-P.; Wu, H.; Wang, H.-J.; Duan, Y.-X.; Zhang, J.-M. Cellulose Nanocrystals-mediated Phase Morphology of PLLA/TPU Blends for 3D Printing. *Chin. J. Polym. Sci.* **2022**, *40*, 299–309. [CrossRef]
139. Bardot, M.; Schulz, M.D. Biodegradable Poly(Lactic Acid) Nanocomposites for Fused Deposition Modeling 3D Printing. *Nanomaterials* **2020**, *10*, 2567. [CrossRef]
140. Dalloul, F.; Mietner, J.B.; Navarro, J.R.G. Production and 3D Printing of a Nanocellulose-Based Composite Filament Composed of Polymer-Modified Cellulose Nanofibrils and High-Density Polyethylene (HDPE) for the Fabrication of 3D Complex Shapes. *Fibers* **2022**, *10*, 91. [CrossRef]
141. Liang, J.-Z. Effects of tension rates and filler size on tensile properties of polypropylene/graphene nano-platelets composites. *Compos. Part B Eng.* **2019**, *167*, 241–249. [CrossRef]
142. Ding, W.; Kuboki, T.; Wong, A.; Park, C.B.; Sain, M. Rheology, thermal properties, and foaming behavior of high d-content polylactic acid/cellulose nanofiber composites. *RSC Adv.* **2015**, *5*, 91544–91557. [CrossRef]
143. Santamaria-Echart, A.; Arbelaiz, A.; Saralegi, A.; Fernández-D'Arlas, B.; Eceiza, A.; Corcuera, M.A. Relationship between reagents molar ratio and dispersion stability and film properties of waterborne polyurethanes. *Colloids Surf. A Physicochem. Eng. Asp.* **2015**, *482*, 554–561. [CrossRef]
144. Saralegi, A.; Rueda, L.; Martin, L.; Arbelaiz, A.; Eceiza, A.; Corcuera, M. From elastomeric to rigid polyurethane/cellulose nanocrystal bionanocomposites. *Compos. Sci. Technol.* **2013**, *88*, 39–47. [CrossRef]
145. Ultimate Materials Guide—3D Printing Flexible Filament. 2022. Available online: https://www.simplify3d.com/support/materials-guide/flexible/ (accessed on 8 November 2022).

146. Direct Drive vs Bowden Extruder: The Differences. All3DP. 2022. Available online: https://all3dp.com/2/direct-vs-bowden-extruder-technology-shootout/ (accessed on 8 November 2022).
147. Larraza, I.; Vadillo, J.; Calvo-Correas, T.; Tejado, A.; Olza, S.; Peña-Rodríguez, C.; Arbelaiz, A.; Eceiza, A. Cellulose and Graphene Based Polyurethane Nanocomposites for FDM 3D Printing: Filament Properties and Printability. *Polymers* **2021**, *13*, 839. [CrossRef] [PubMed]
148. Frone, A.N.; Ghiurea, M.; Nicolae, C.A.; Gabor, A.R.; Badila, S.; Panaitescu, D.M. Poly(lactic acid)/Poly(3-hydroxybutyrate) Bi-ocomposites with Differently Treated Cellulose Fibers. *Molecules* **2022**, *27*, 2390. [CrossRef] [PubMed]
149. Bi, H.; Ren, Z.; Ye, G.; Sun, H.; Guo, R.; Jia, X.; Xu, M. Fabrication of cellulose nanocrystal reinforced thermoplastic polyurethane/polycaprolactone blends for three-dimension printing self-healing nanocomposites. *Cellulose* **2020**, *27*, 8011–8026. [CrossRef]
150. Kumar, V.; Singh, R.; Ahuja, I. Secondary recycled acrylonitrile–butadiene–styrene and graphene composite for 3D/4D applications: Rheological, thermal, magnetometric, and mechanical analyses. *J. Thermoplast. Compos. Mater.* **2020**, *35*, 761–781. [CrossRef]
151. Kaynan, O.; Yildiz, A.; Bozkurt, Y.E.; Yenigun, E.O.; Cebeci, H. Development of Multifunctional CNTs Reinforced PEI Filaments for Fused Deposition Modeling. In Proceedings of the AIAA Scitech 2019 Forum, San Diego, CA, USA, 7–11 January 2019.
152. Bilkar, D.; Keshavamurthy, R.; Tambrallimath, V. Influence of carbon nanofiber reinforcement on mechanical properties of polymer composites developed by FDM. *Mater. Today Proc.* **2021**, *46*, 4559–4562. [CrossRef]
153. Kim, N.P. 3D-Printed Conductive Carbon-Infused Thermoplastic Polyurethane. *Polymers* **2020**, *12*, 1224. [CrossRef]
154. Moola, A.R.; Santo, J.; Penumakala, P.K. Multiscale analysis for predicting elastic properties of 3D printed polymer-graphene nanocomposites. *Mater. Today Proc.* **2022**, *62*, 4025–4029. [CrossRef]
155. Rinaldi, M.; Bragaglia, M.; Nanni, F. Mechanical performance of 3D printed polyether-ether-ketone nanocomposites: An experimental and analytic approach. *Compos. Struct.* **2023**, *305*, 116459. [CrossRef]
156. Sheikh, T.; Behdinan, K. Insight of Discrete Scale and Multiscale Methods for Characterization of Composite and Nanocomposite Materials. *Arch. Comput. Methods Eng.* **2022**, *30*, 1231–1265. [CrossRef]
157. Behdinan, K.; Moradi-Dastjerdi, R.; Safaei, B.; Qin, Z.; Chu, F.; Hui, D. Graphene and CNT impact on heat transfer response of nanocomposite cylinders. *Nanotechnol. Rev.* **2020**, *9*, 41–52. [CrossRef]
158. Moradi-Dastjerdi, R.; Behdinan, K.; Safaei, B.; Qin, Z. Buckling behavior of porous CNT-reinforced plates integrated between active piezoelectric layers. *Eng. Struct.* **2020**, *222*, 111141. [CrossRef]
159. Moradi-Dastjerdi, R.; Behdinan, K. Dynamic performance of piezoelectric energy harvesters with a multifunctional nanocomposite substrate. *Appl. Energy* **2021**, *293*, 116947. [CrossRef]
160. Moradi-Dastjerdi, R.; Behdinan, K. Free vibration response of smart sandwich plates with porous CNT-reinforced and piezoelectric layers. *Appl. Math. Model.* **2021**, *96*, 66–79. [CrossRef]
161. Sheikh, T.; Behdinan, K. Novel experimental and multiscale study of additively manufactured ABS-carbon nanotubes nanocomposites. *Appl. Mater. Today* **2023**, *35*, 101963. [CrossRef]
162. Nasirov, A.; Gupta, A.; Hasanov, S.; Fidan, I. Three-scale asymptotic homogenization of short fiber reinforced additively manufactured polymer composites. *Compos. Part B Eng.* **2020**, *202*, 108269. [CrossRef]
163. Nasirov, A.; Fidan, I. Prediction of mechanical properties of fused filament fabricated structures via asymptotic homogenization. *Mech. Mater.* **2020**, *145*, 103372. [CrossRef]
164. Qadri, A.M.; Singh, G.K.; Paul, D.; Gupta, T.; Rabha, S.; Islam, N.; Saikia, B.K. Variabilities of δ13C and carbonaceous components in ambient PM2.5 in Northeast India: Insights into sources and atmospheric processes. *Environ. Res.* **2022**, *214*, 113801. [CrossRef]
165. Qadri, A.; Rabha, S.; Saikia, B.; Gupta, T. Seasonal and episodic influence of local meteorology on fine particulate matter at a regional background site in North East India. In Proceedings of the EGU21, Online, 19–30 April 2021. [CrossRef]
166. Izhar, S.; Gupta, T.; Qadri, A.M.; Panday, A.K. Wintertime chemical characteristics of aerosol and their role in light extinction during clear and polluted days in rural Indo Gangetic plain. *Environ. Pollut.* **2021**, *282*, 117034. [CrossRef]